View metadata, citation and similar papers at core.ac.uk

brought to you by CORE

provided by Bradford Scholars

UNIVERSITY of BRADFORD

Library

The University of Bradford Institutional Repository

http://bradscholars.brad.ac.uk

This work is made available online in accordance with publisher policies. Please refer to the repository record for this item and our Policy Document available from the repository home page for further information.

To see the final version of this work please visit the publisher's website. Access to the published online version may require a subscription.

Link to original published version: *http://dx.doi.org/10.1016/j.compchemeng.2015.05.022*

Citation: Barello M, Manca D, Patel R and Mujtaba IM (2015) Operation and modelling of RO desalination process in batch mode. Computers and Chemical Engineering. 83: 139-156.

Copyright statement: © 2015 Elsevier Ltd. Full-text reproduced in accordance with the publisher's self-archiving policy.

This manuscript version is made available under the CC-BY-NC-ND 4.0 license *http://creativecommons.org/licenses/by-nc-nd/4.0/*

M. Barello*, D. Manca*, R. Patel and I.M. Mujtaba****

***PSE-Laboratory - Dipartimento di Chimica, Materiali e Ingegneria Chimica "G. Natta", Politecnico di Milano, Piazza Leonardo da Vinci 32, 20133 Milan, Italy. davide.manca@polimi.it

**Chemical Engineering Division, School of Engineering, University of Bradford, Richmond Road, Bradford,
West Yorkshire, BD7 1DP, UK. r.patel@bradford.ac.uk, I.M.Mujtaba@bradford.ac.uk

Abstract

The performance of a batch reverse osmosis (RO) desalination process in terms of permeate quantity and salinity as a function of feed pressure and feed salinity is evaluated by using laboratory experiments and process modelling. Special attention is paid to the water and salt permeability constants (K_w, K_s) which affect the permeate and salt flux across the membrane. K_w and K_s are found to be strongly pressure-dependent for the batch system which is in-line with earlier observations for continuous RO systems. However, the most important findings of this work are the dependence of K_w and K_s on feed salinity, something that have never been observed or reported in the literature. In order to better qualify these observations, further experiments with the batch system are conducted with a constant feed salinity so that the operating condition resembles that of a continuous RO process.

Keywords: Reverse osmosis; Batch system; Pilot plant; Performance assessment.

1. Introduction

Desalination via reverse osmosis (RO) is a separation process for making fresh water from seawater, and has increased in popularity over the last few years. Its popularity comes from the fact that it has some advantages in terms of saving energy, modularity, flexibility, small plant sizes, or even less installation space compared to other traditional techniques, which include thermal processes, such as the multistage flash (MSF) distillation (Schiffler, 2004). Most reverse osmosis (RO) and nanofiltration (NF) processes operate as plug-flow (PF) systems in continuous mode. In these processes, permeate recovery, flux and cross flow are coupled. They are ideal for purification of pre-treated source waters of uniform composition with limited permeate recovery percentages. Nevertheless, some authors are focusing on an emerging new semi batch technique (Stover, 2011). The volume of concentrate produced is less in a batch RO, with little membrane fouling or scale deposition (Tarquin and Delgado, 2012). However, the application of batch operation to RO and NF has been limited because they require higher energy input and the permeate is also characterized by a lower quality. Lately, a novel semi-batch process applicable for either RO or NF plants is becoming more attractive. In these semi-batch systems, the brine feed is recirculated to the feed tank until the target permeate recovery amount is reached. The process is then stopped and the vessel drained. The performances of these

processes are better in terms of high adjustable recovery rates that result in the decrease of concentrate production and source water pumping. Some other conveniences in using these semi-batch plants are the independently adjustable cross-flow and there is less evidence of the fouling and scaling phenomena. In addition, they consume less energy and require fewer membrane elements than PF systems.

In RO process, Djebedjian *et al.* (2008) observed pressure dependency on the permeate salinity. Voros *et al.* (1996) also noted dependency of water and salt permeability constants on pressure. Al-Bastaki and Abbas (2004) observed dependency of water permeability constants on fouling. While Du et al. (2014) considered only temperature dependent water permeability constant, Kim et al. (2013) just used a single value for water permeability constant. None of these studies considered the effect of feed salinity on water and salt permeability constants which is one of the objectives of this work. In addition, none of the previous studies (although limited) focused on the development of a batch RO process model validated against experimental data which is another objective of this work.

In this work, a batch operation of a RO desalination plant is considered. The batch system is characterized by the recirculation of the rejected brine into the feed tank. First, the performance of the plant is assessed by studying the influence of some operating parameters, such as operating pressure and feed salinity, on the permeate quantity and permeate salinity. Particular attention is paid to understand the influence of the operating conditions (*i.e.* pressure and feed salinity) on the water permeability constant (K_w). In this respect, two literature models are used. Second, the dynamic concentration polarization (CP) mechanism is studied, as CP is one of the important parameters affecting the performance of an RO process (Meares, 1976). Third, salt transport phenomenon across the membrane is analyzed by evaluating the pressure and feed salinity influence on salt permeability constant and salt mass flow and compared with those observed in the literature. Fourth, a system of differential and algebraic equations is proposed to model the batch system, which is validated using the experimental data. Finally, In order to better quantify the batch performances and to qualify the dependence of water permeability constant on feed salinity some other experiments were conducted in a constant feed concentration mode. Permeate quantity, salinity, water permeability, concentration polarization, salt permeability and salt mass flow are then compared with those obtained under variable feed concentration mode.

2. Experimental Set-up and Method

Figure 1 shows a schematic view of the RO pilot plant used for the experiments. A couple of triple-plunger-positive-displacement pumps (Pump 1 and Pump 2) located within the stainless steel cabinet, and driven by a two-speed electric motor are used to pump the liquid. The pumps and motor drive are mounted on a bedplate, which in turn is mounted on vibration absorbing dampers. The pumps are connected together by a flexible coupling so that both can be run simultaneously. A three-way ball valve (V3) situated at the rear of the unit is used to divert the outlet flow from pump no. 2 to the suction of pump no. 1, for instances when only flow from pump no. 1 is required.

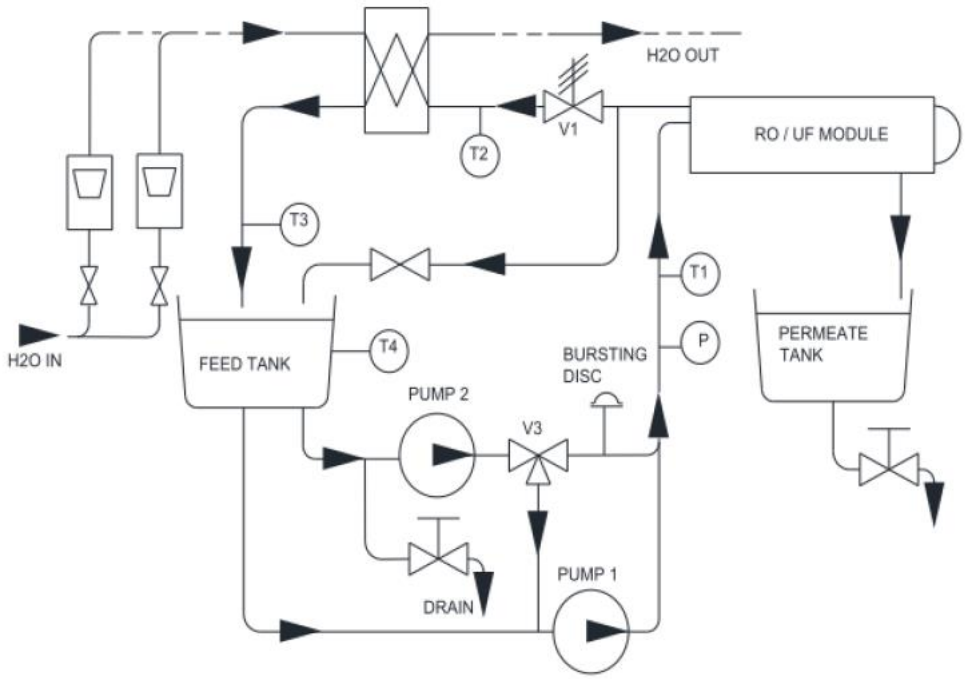

Figure 1. Experimental apparatus for RO. (Courtesy of Armfield)

Liquid from the feed tank is pressurized and pumped through the membrane holder module which contains two tubular membranes in series (Armfield FT18). Upon leaving the module, part of the solution then passes through a plate heat exchanger before being discharged back into the feed tank. Work done on the fluid, by the pumps, causes a gradual increase in temperature, with time. This is avoided by pumping the fluid through plate heat exchanger where it is cooled by water. The cooling water flow is controlled manually and flow rates are monitored on variable-area flow meters. The other part of the solution is directly passed to the feed tank. This completes the closed loop recycle system. The permeate drains by gravity into a dedicated permeate tank.

Figure 2 shows a simpler schematic diagram of the process. In order to study the influence of the operating parameters on the performance of the RO process, experiments were carried out at two different operating pressures and three different initial feed salinities. The operating pressure is kept constant by manually adjusting valve (V1) during the course of experiments. Each set of experiments was carried out for 8 hours and the permeate quantity, permeate salinity, and permeate total salinity were measured every 15 or 30 minutes. A calibrated conductivity meter was used to measure the salinity. Figure 3 shows the calibration curve.

It is assumed that the feed and the permeate tank are well mixed. As the experiments were carried out with clean membranes there was no fouling consideration in this work. As the experimental set-up facilitates only few measurements such as permeate conductivity and permeate rate, some simple mass balance equations are developed to calculate the remaining parameter of the process.

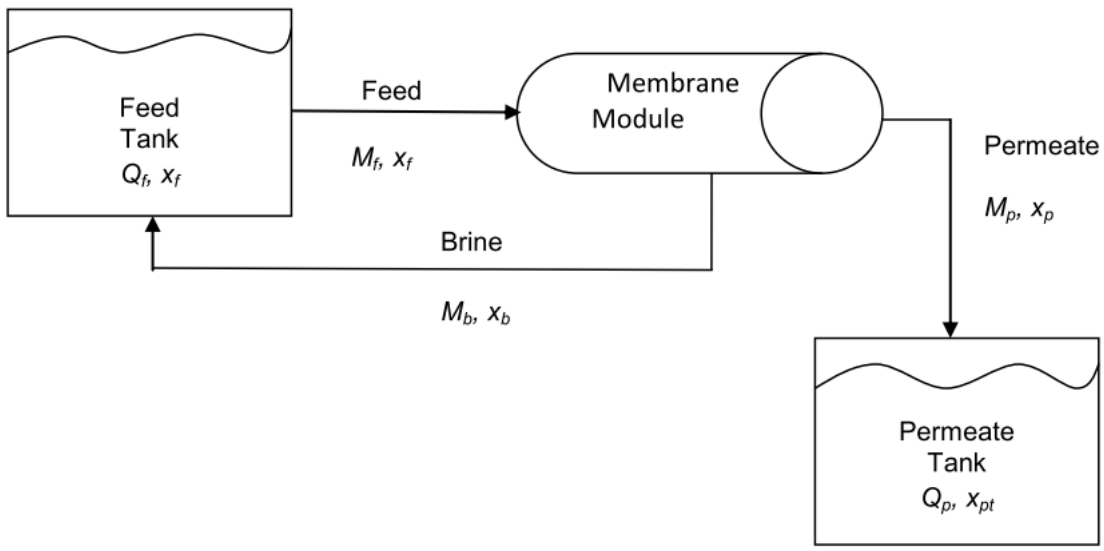

Figure 2. Schematic diagram of batch RO process.

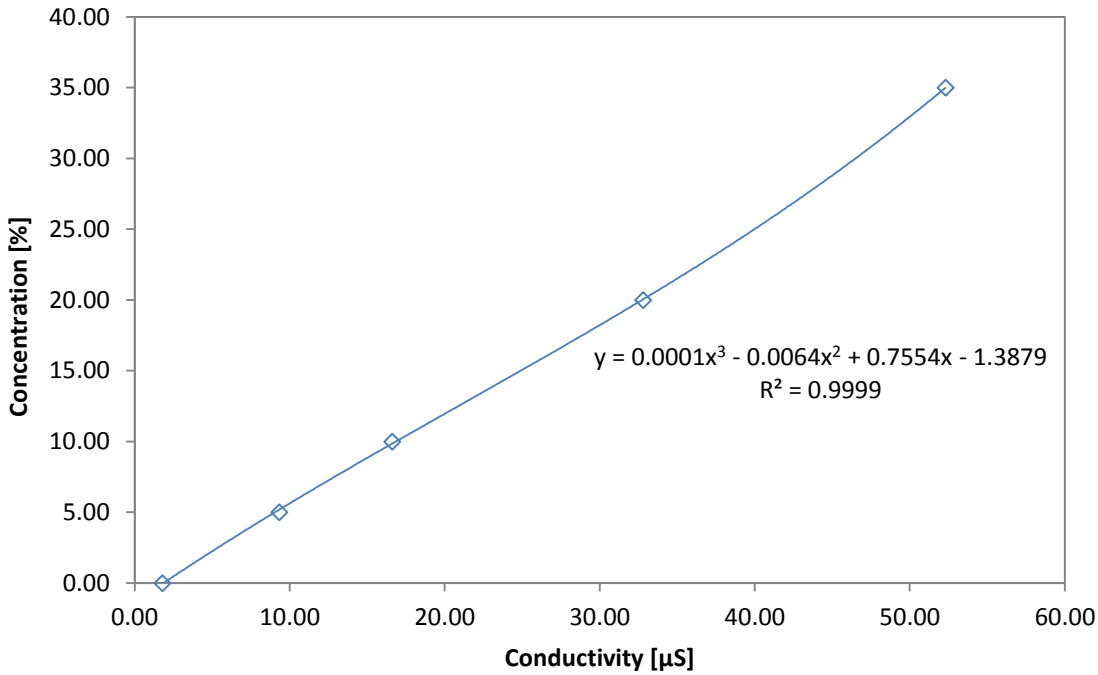

Figure 3. Salinity-Conductivity calibration curve [Concentration is in g salt/L water]

For each time interval, a mass balance was carried out in order to calculate the salinity in the feed tank (x_f) because it was difficult to make meaningful measurements with the conductivity meter due to vibrations, mixing and recirculation of the brine feed.

The overall mass balances are given by the following equations:

$$Q_f^t = Q_f^{t-\Delta t} - M_p \Delta t \quad (1)$$

Where, Q_f^t is the feed quantity at time t, $Q_f^{t-\Delta t}$ is the feed quantity at time (t-Δt) and M_p is the permeate flow rate between the time (t-Δt) and (t).

$$Q_p^t = Q_p^{t-\Delta t} + M_p \Delta t \quad (2)$$

Where, Q_p^t is the total permeate quantity at time *t*, $Q_p^{t-\Delta t}$ is the feed quantity at time (*t*-Δ*t*)

Salinity balances:

$$Q_f^t x_f^t = Q_f^{t-\Delta t} x_f^{t-\Delta t} - M_p x_p \Delta t \quad (3)$$

Where, x_f^t is the feed salinity at time *t*, $x_f^{t-\Delta t}$ is the feed salinity at time (*t*-Δ*t*) and x_p is the instantaneous permeate salinity at time *t*

$$Q_p^t x_{pt}^t = Q_p^{t-\Delta t} x_{pt}^{t-\Delta t} + M_p x_p \Delta t \quad (4)$$

Where, x_{pt}^t and $x_{pt}^{t-\Delta t}$ are the accumulated permeate salinity at time *t* and (*t*-Δ*t*) respectively.

Equations (1) and (2) give:

$$Q_f^t + Q_p^t = Q_f^{t-\Delta t} + Q_p^{t-\Delta t} \quad (5)$$

Whilst Equations (3) and (4) give:

$$Q_f^t x_f^t + Q_p^t x_{pt}^t = Q_f^{t-\Delta t} x_f^{t-\Delta t} + Q_p^{t-\Delta t} x_{pt}^{t-\Delta t} \quad (6)$$

Equations (5) and (6) can be used to calculate Q_f^t and x_f^t respectively at any given time *t*. With values of initial feed tank quantity and concentration and measurements of permeate tank quantity and concentration at regular intervals, Equations (1) and (2) can be used to calculate the quantity and concentration of feed tank.

Table 1. Membrane Properties and Experimental Data

Membrane	AFC99
A [m^2]	0.024
L [m]	0.3
d_h [m]	0.01635
Q_0 [L]	8
x_0 [g/L]	33-23-13
Δt [min]	30-15
M_f [l/min]	18
ΔP [bar]	40-45

Table 1 lists membrane type, membrane area, membrane length, membrane diameter, initial feed quantity, initial feed salinity, step time, feed flow rate, and pressure difference across the membrane. Note, although explicit pressure drop models are available for Filmtec membrane modules in the literature (Altaee, 2012), for simplicity, pressure drop in the membrane system used in this work is built in ΔP.

3. Experimental results

3.1 Permeate flux

Figure 4 shows the permeate flux trend whilst Figure 5 shows the corresponding feed tank salinity for a given pressure for two different operating pressures and an initial feed salinity of 25 g/L. The decrease in permeate flux is due to the increase in feed salinity with time. The separation becomes

more difficult because an increase in x_f means an increase in the osmotic pressure on the feed solution side resulting in a decrease of the net driving force (ΔP-$\Delta\pi$). Also, higher pressures; correspond to higher permeate flux, due to higher driving force and M_p is directly proportional to the pressure. This leads to high values of x_f at any given time at higher pressure (Fig. 5). A similar trend was found for x_{f0} of 35 and 15 g/L. This behaviour of the permeate flux at different pressures confirms the findings of Shamel and Chung (2006) and Djebedjian *et al.* (2008). However, it is to be noted that the slopes of the M_p profiles (Figure 4) at two different pressures are different but is linked to x_f profiles shown in Figure 5. The x_f profile at higher pressure is steeper than at lower pressure leading to steeper M_p profile at higher pressure.

Figure 6 shows the influence of initial feed salinity on the permeate flux at a constant pressure of 40 bar. Higher values of the feed salinity correspond to reduced amount of permeate flux because the separation becomes more difficult corresponding to an increasing of the feed tank salinity as shown in Figure 5. Same results were collected for an operating pressure of 45 bar. Similar trends are reported by Shamel and Chung (2006), Djebedjian *et al.* (2008) and Wilf and Klinko (1994). However, it is to be noted that M_p profiles (Figure 6) at different initial feed salinity are different. Although for x_{f0} = 15 and 25, the slopes are nearly the same, it is different for x_{f0} = 35. It certainly reveals that for a given feed pressure there is a limit to initial feed salinity, and it is due to the fact that higher initial feed salinity leads to steeper x_p profile (Figure 8), therefore steeper x_f profile leading to steeper decrease in osmotic pressure difference making M_p profile less steeper (as evidenced in Figure 6).

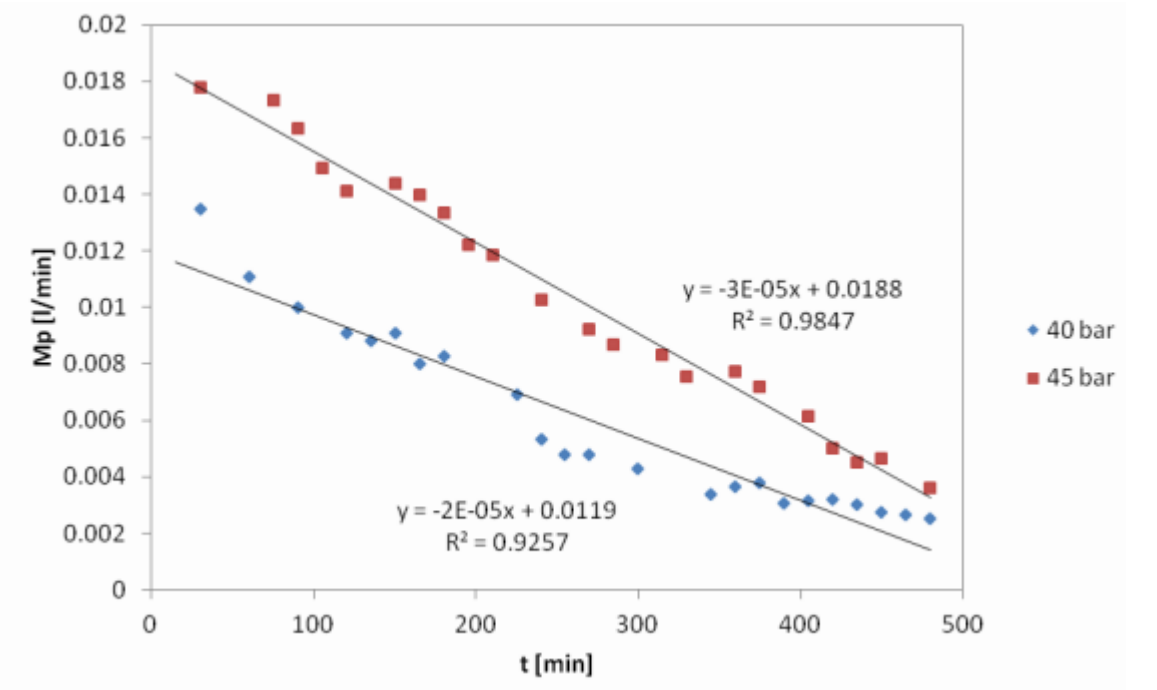

Figure 4. Permeate flux trend with x_{f0}=25 g/L.

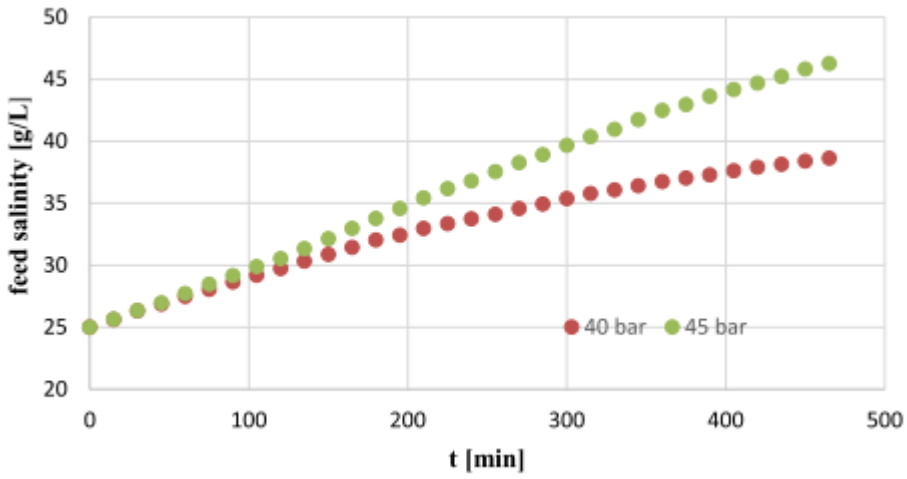

Figure 5. Feed tank salinity trend with x_{f0}=*25* g/L.

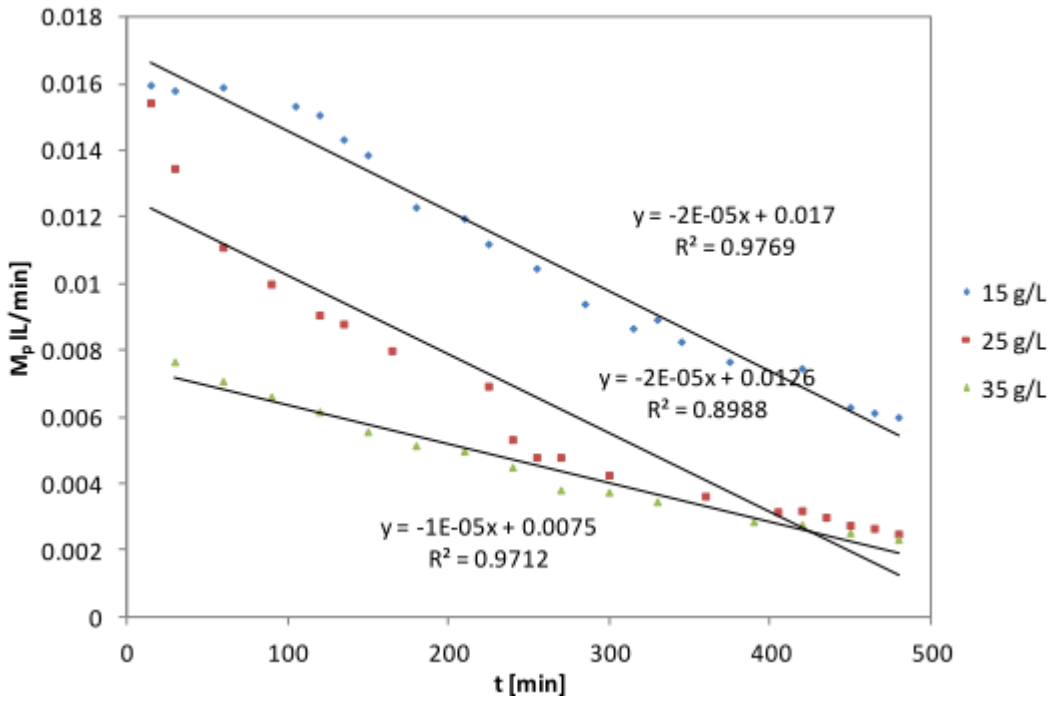

Figure 6. Permeate flux with *P=40* bar.

3.2 Permeate salinity

Figure 7 shows instantaneous permeate salinity dynamic evolution for initial feed salinity of 15 g/L, at two operating pressures (40 and 45 bar). The permeate salinity increases gradually almost at the same pace for both pressures, with increase in feed salinity until about 250 min. Beyond 250 min the rate of increase of permeate salinity at 45 bar is greater than that at 40 bar. This is probably because beyond 250 min, the effects of higher pressure are greater than the effect of concentration polarization (*CP*, explained later in this paper) and lets more salt into the permeate. The same behaviour was found for initial salinity values of 25 and 35 g/L. These results confirm the findings of Shamel and

Chung (2006), Djebedjian *et al.* (2008) and Voros *et al.* (1996). Figure 8 shows how higher initial feed salinities result in higher permeate salinities for an operating pressure of 45 bar. Similar trends were found at 40 bar.

3.3 Effect of feed salinity

Figure 9 shows the variation of permeate salinity with the feed salinity at a constant pressure of 40 bar (similar trends were obtained at 45 bar). Figure 10 shows the variation of M_p with x_f at different initial conditions, x_{f0}. In an ideal case, one would expect all the points in Figure 9 falling on a single line. However, beyond x_f=25, the rate of increase in x_p is higher for x_{f0}=15 compared to that for x_{f0}=25. This is due to the fact that with x_{f0}=15 the *CP* effect becomes increasingly more pronounced as feed salinity increases. This reduces the permeate flow (Figure 10) and leads to an increase in the permeate salinity for the same passage of salt through the membrane (note that salt passage also gradually increases with increasing feed salinity for a given pressure, see discussion in Section 6). However, when x_{f0}=25, the *Mp* is higher compared to that at x_f=27 (with x_{f0}=15; see Figure 10), which consequently decreases the value of x_p (see Figure 9). A similar explanation can be given, to the behaviour of the profiles with x_{f0}=35 and x_{f0}=25. To the best of the authors' knowledge, these types of observations have been neither made nor reported in the literature. Section 4 captures further the effect of initial feed salinity.

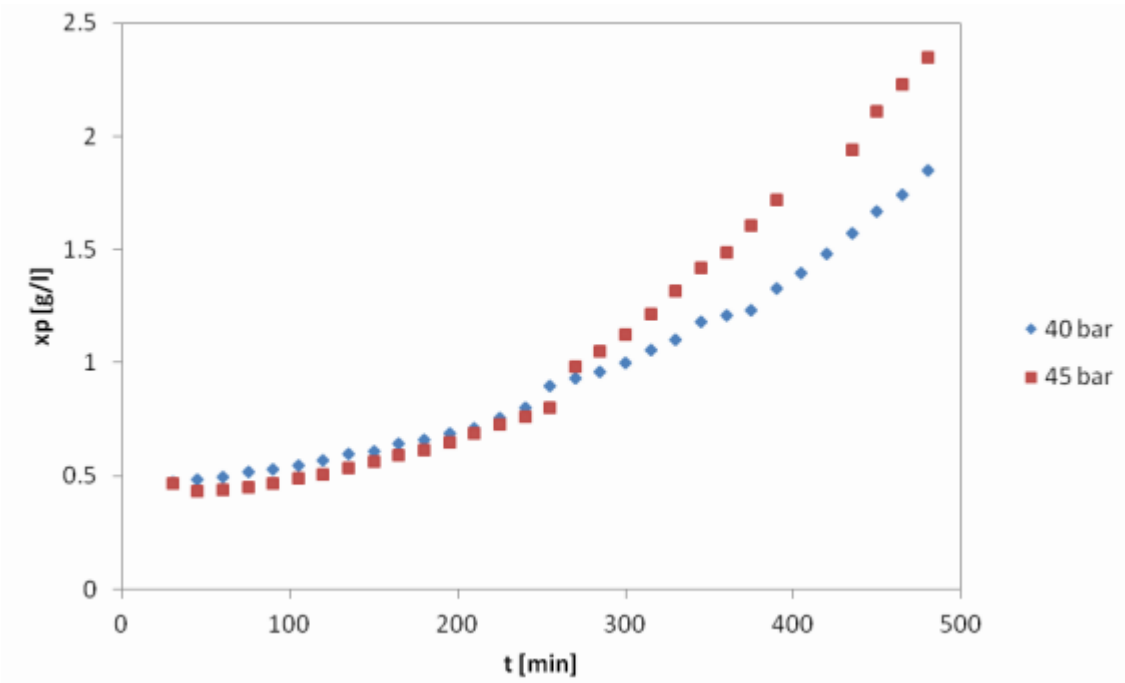

Figure 7. Permeate salinity trend with *xf0=15* g/L.

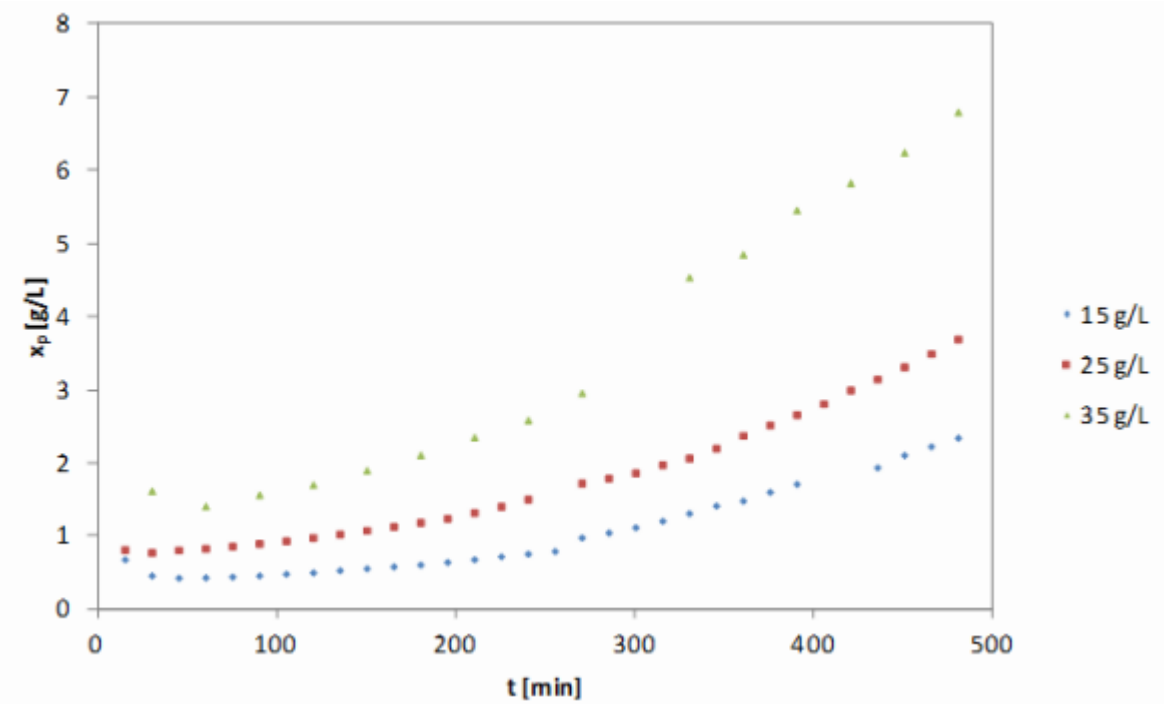

Figure 8. Permeate salinity trend at *P=45* bar.

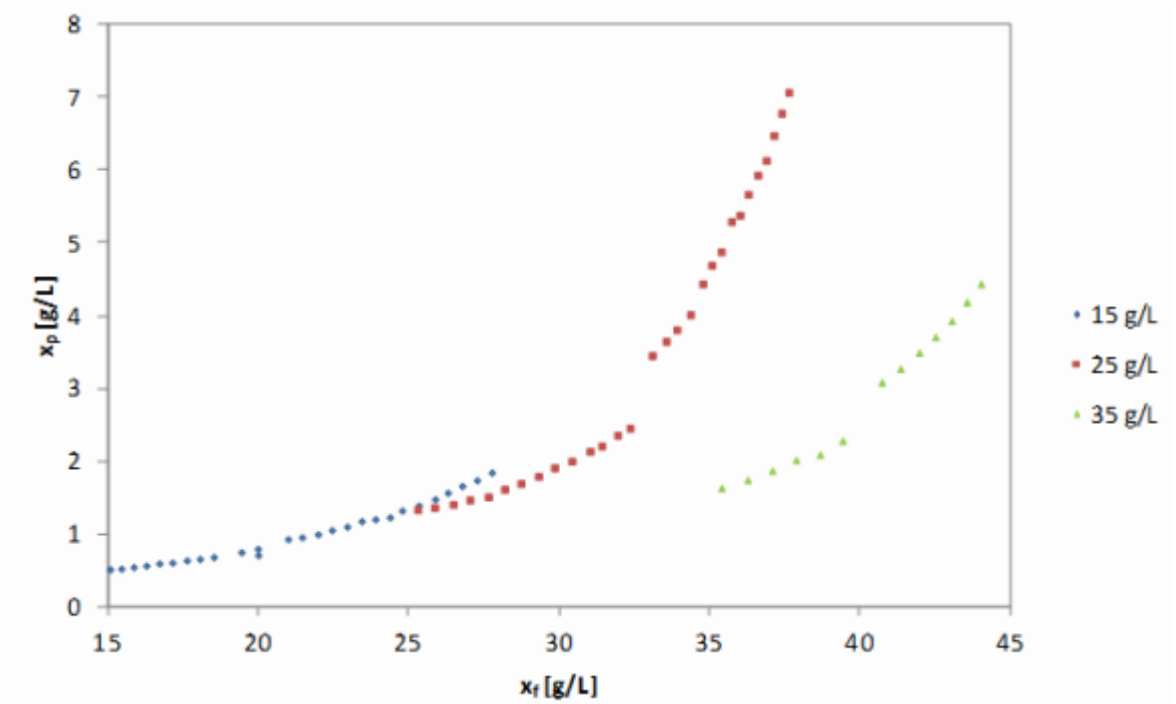

Figure 9**.** Permeate salinity variation with the feed salinity at *P=40* bar.

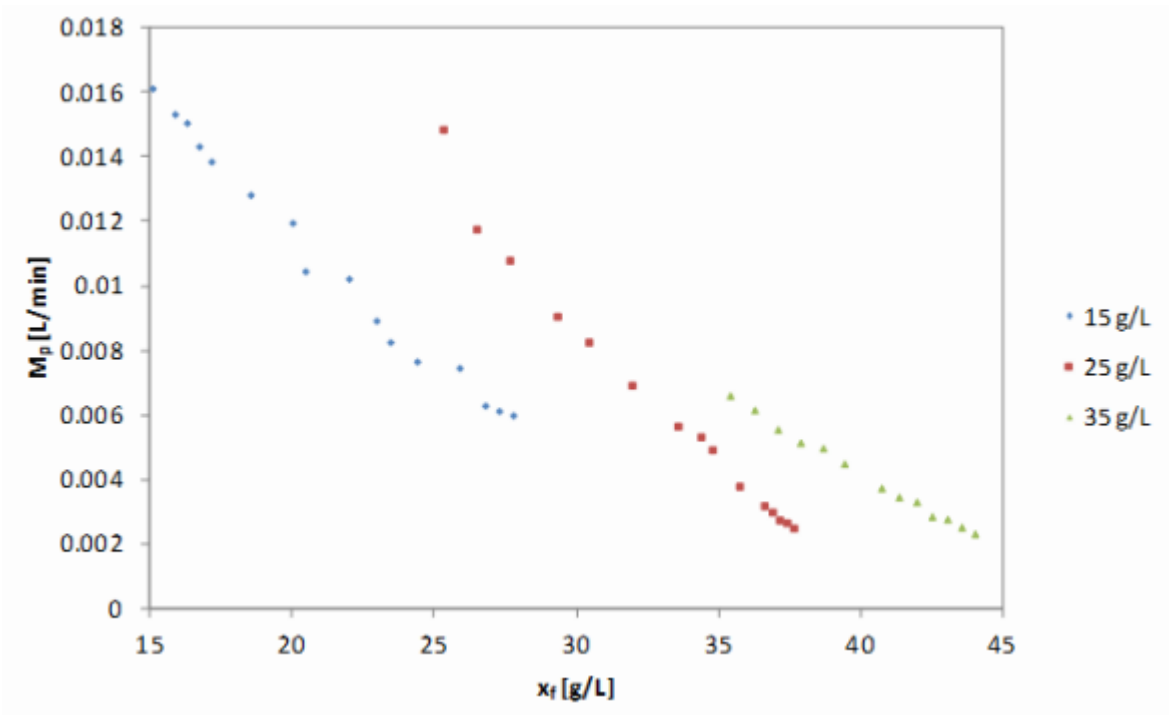

Figure 10. Permeate flux variation with the feed salinity at *P=40* bar.

4. Water permeability calculations

One of the parameters that greatly affects the performance of a RO plant, is the water permeability constant, because it is directly proportional to the permeate flux and inversely proportional to the driving force of the process. In order to calculate the driving force the methods used by El-Dessouky and Ettouney (2002) and Meares (1976) are considered

4.1 El-Dessouky and Ettouney (2002) model

According to the widely used solution-diffusion model, the water flux through the membrane is given by

$$M_p = K_w \left(\Delta P - \Delta\pi\right) A C_1 \tag{7}$$

Where C_1 is a conversion factor (=1000 L/m^3), K_w the water permeability, A the membrane area, ΔP the pressure difference between the feed and permeate sides of the membrane and $\Delta\pi$ the osmotic pressure difference across the membrane.

Equations (8) and (9) enable the calculation of the brine flow rate and the brine salinity (Figure 2).

$$M_b = M_f - M_p \tag{8}$$

$$x_b = \frac{M_f x_f - M_p x_p}{M_b} \tag{9}$$

Where M_b, M_f and M_p are the brine, feed and permeate flux respectively.

It is thus possible to calculate the permeate osmotic pressure (Equation (10)), the feed osmotic pressure (Equation (12)) and the brine osmotic pressure (Equation (11)), in order to obtain the net osmotic pressure differential across the membrane ($\Delta\pi$) through Equation (14). For the solute salinity considered in this work, the osmotic pressure is approximately a linear function of solute salinity for simplicity. These correlations are similar (multiplying factor is 0.7584) to those used by El-Dessouky and Ettouney (2002) for salinity up to 42 g/L and to those used by Geraldes et al. (2001) who suggested a multiplying factor of 0.8051 for salinity up to 90 g/L. In addition, Wardeh and Morvan (2008) used the same correlation of Geraldes et al. for a detailed CFD (Computational Fluid Mechanics) based simulation of RO desalination process. Note, however, a nonlinear correlations for salinity up to 48 g/l has been suggested by Lu et al. (2007).

$$\pi_p = 0.7579 x_p \tag{10}$$

$$\pi_b = 0.7579 x_b \tag{11}$$

$$\pi_f = 0.7579 x_f \tag{12}$$

$$\bar{\pi} = 0.5(\pi_f + \pi_b) \tag{13}$$

$$\Delta\pi = \bar{\pi} - \pi_p \tag{14}$$

Finally, it is possible to calculate the water permeability coefficient K_w using Equation (15).

$$K_w = \frac{M_p}{\left(\Delta P - \Delta\pi\right) AC_1} \tag{15}$$

Figure 11 shows the water permeability coefficient at two different levels of pressure with an initial feed salinity of 25 g/L. It is possible to observe how its value increases at higher pressures due to a higher driving force. Experiments conducted with an initial feed salinity of 15 and 35 g/L show a similar dependence.

Figure 12 shows a rather important finding i.e. the effect of the feed salinity on the water permeability constant which has not been reported in the literature prior to this work. Some authors, who studied the dependence on $K_{w,}$ focused only on the pressure (Voros et al., 1996) or its decay with the time due to the fouling phenomenon (Zhu et al., 1997) and (Al-Bastaki and Abbas, 2004). In this work, we observed that K_w values depend on feed salinity (see also Barello *et al.*, 2014) and a higher feed salinity corresponds to a smaller water permeability coefficient. This trend confirms the dependence found between the permeate flux and the initial feed salinity at both operating pressures. In order to better clarify this dependence, Figure 13 shows the variation of K_w as a function of the feed salinity and the linear regression line of best-fit approach will be used in the following to model the RO process (see Section 7).

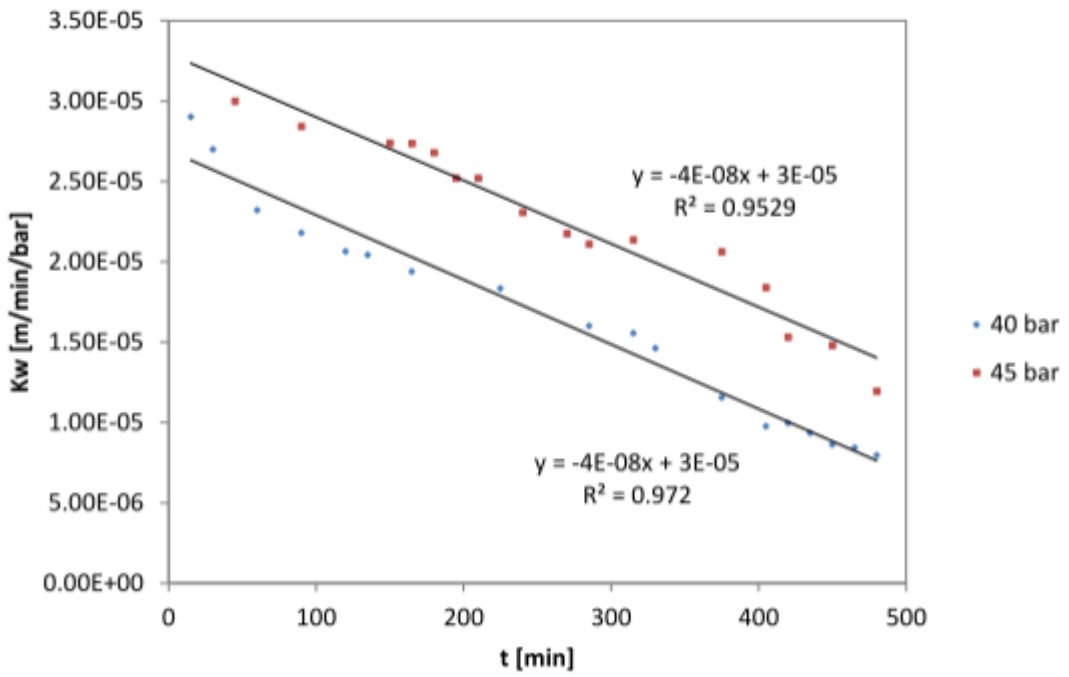

Figure 11. Water permeability trend at x_{f0}=*25* g/L (Note feed salinity continuously increases as it is a batch system)

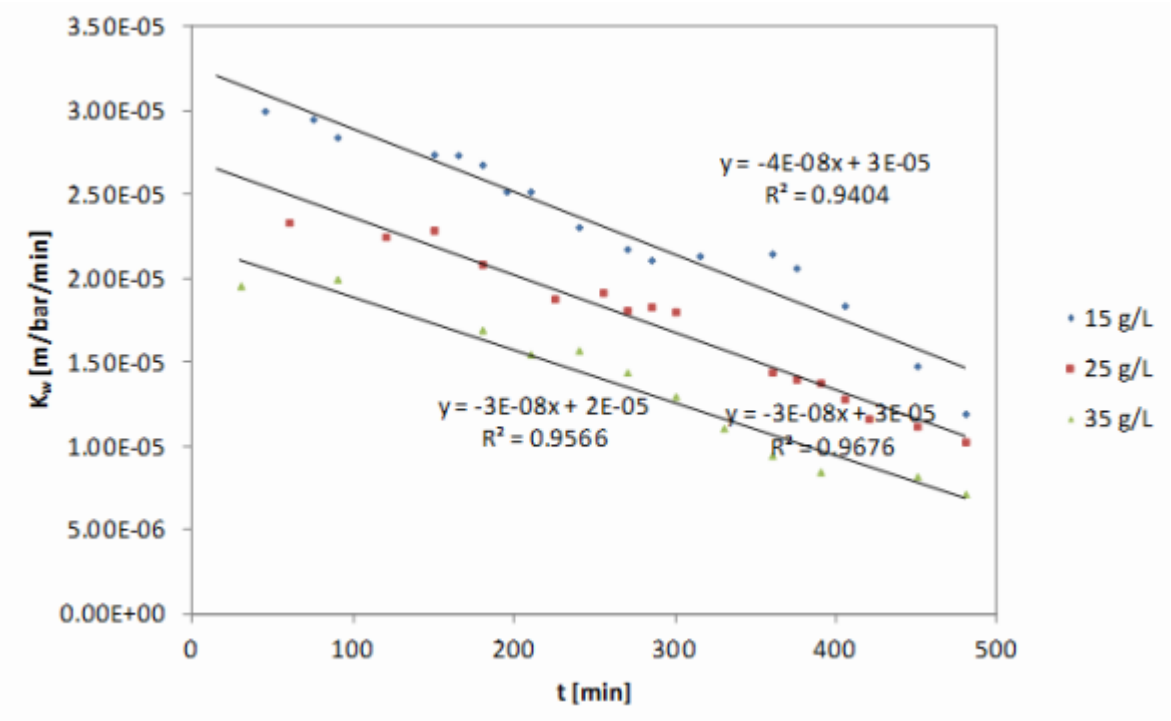

Figure 12. Water permeability trend at *P=45* bar.

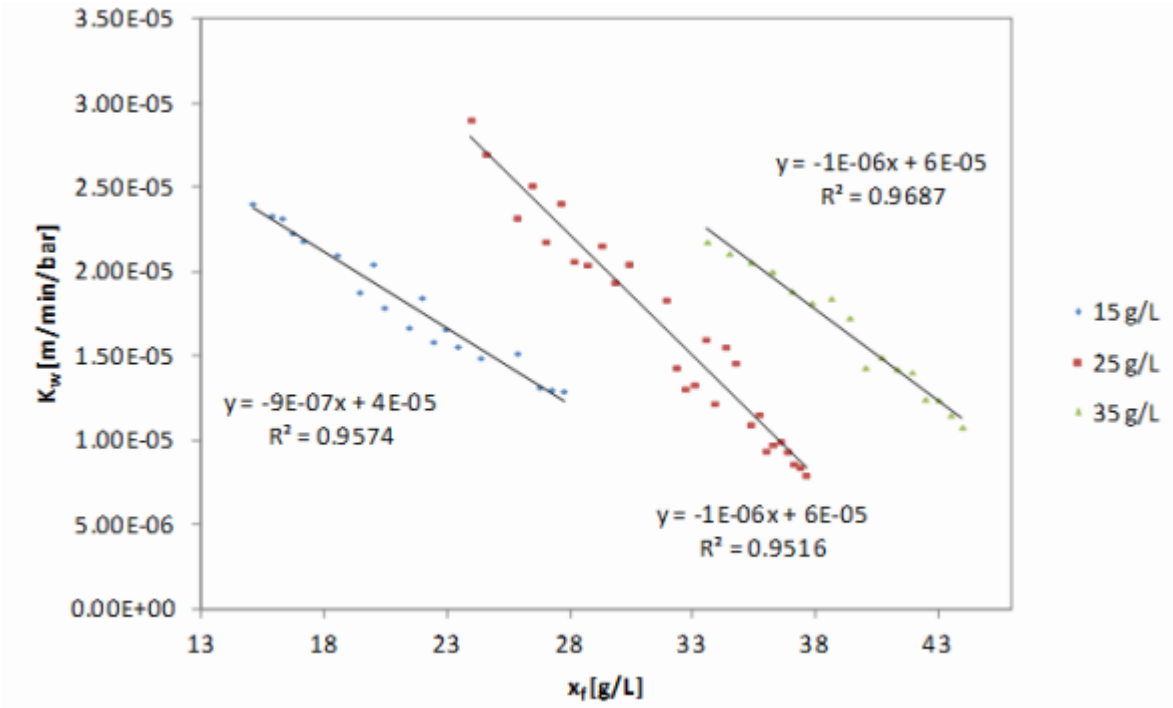

Figure 13. Water permeability trend with feed salinity at *P=40* bar.

4.2 Meares model

Meares (1976) based his reverse osmosis studies on an irreversible thermodynamic treatment of the system. The model assumes turbulent flow, osmotic pressure represented by the Van't Hoff equation, tubular configuration, isothermal conditions, reflection coefficient approximately equal to the intrinsic salt rejection R_j, and the Nerst film model to describe polarization phenomenon.

The permeate flux and the salt rejection are given by:

$$M_p = K_w \left[\Delta P - \left(R_j\right)^2 \alpha R \left(T + 273.15\right) x_w \right] A C_1 \tag{16}$$

$$R_j = \frac{M_p}{M_f} \tag{17}$$

Where α is the number of ions produced on complete dissociation of one molecule of electrolyte, R the universal gas constant and T the temperature. The wall salinity x_w is estimated by:

$$x_w = x_b \frac{\exp\left(\frac{\frac{M_p}{60000A} Sc^{2/3}}{ju}\right)}{R_j + \left(1 - R_j\right)\exp\left(\frac{\frac{M_p}{60000A} Sc^{1/3}}{ju}\right)} \tag{18}$$

Where C_1 is a conversion factor, Sc the Schmidt number, u the brine velocity and j the Chilton-Colburn factor.

$$Sc = \frac{\nu}{D} \tag{19}$$

$$j = 0.0395\,\mathrm{Re}^{-1/4} \tag{20}$$

$$u = \frac{M_b}{60000A} \tag{21}$$

$$Re = \frac{M_f d_h}{\nu A} \tag{22}$$

Where v is the viscosity, d_h the hydraulic diameter of the flow channel and D the diffusivity coefficient. For the physical properties, correlations from Pais *et al.* (2007) are used.

$$\nu = \frac{\mu}{\rho} \tag{23}$$

$$M = 1.0069 - 2.757 \times 10^{-4} T(°C) \tag{24}$$

$$\rho = 498.4M + \sqrt{248400M^2 + 752.4x_f M} \tag{25}$$

$$\mu = 1.234 \times 10^{-6} \exp\left(0.00212x_f + \frac{1965}{273.15 + T}\right) \tag{26}$$

$$D = 6.725 \times 10^{-6} \exp\left(0.154E - 3x_f + \frac{2513}{273.15 + T}\right) \tag{27}$$

In the following figures (Figures 14, 15 and 16), some results are plotted and the trends confirm the various dependences found with the El-Dessouky calculations.

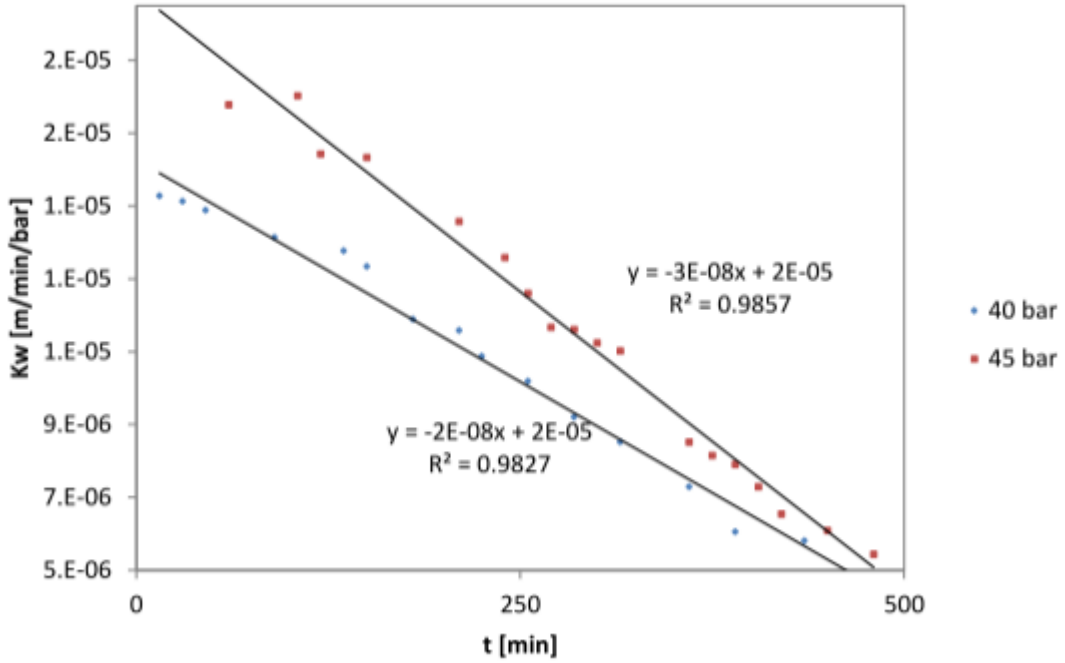

Figure 14. Water permeability trend at x_{f0}=*15 g/L*.

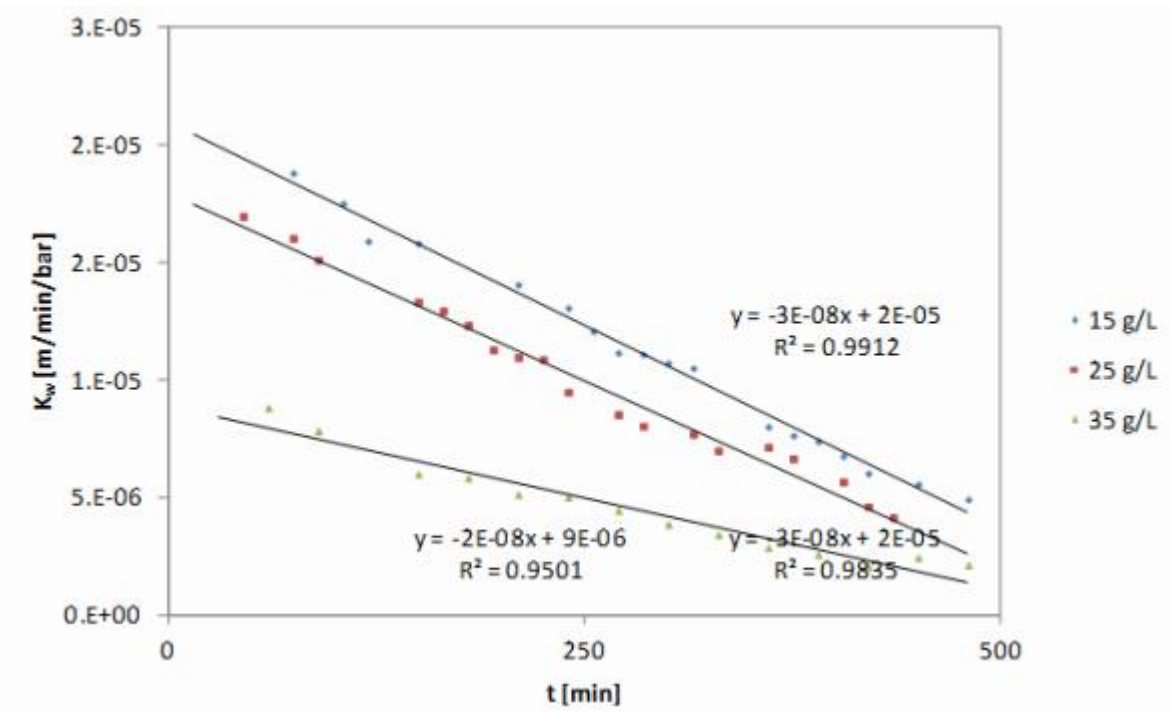

Figure 15. Water permeability trend at *P=40* bar.

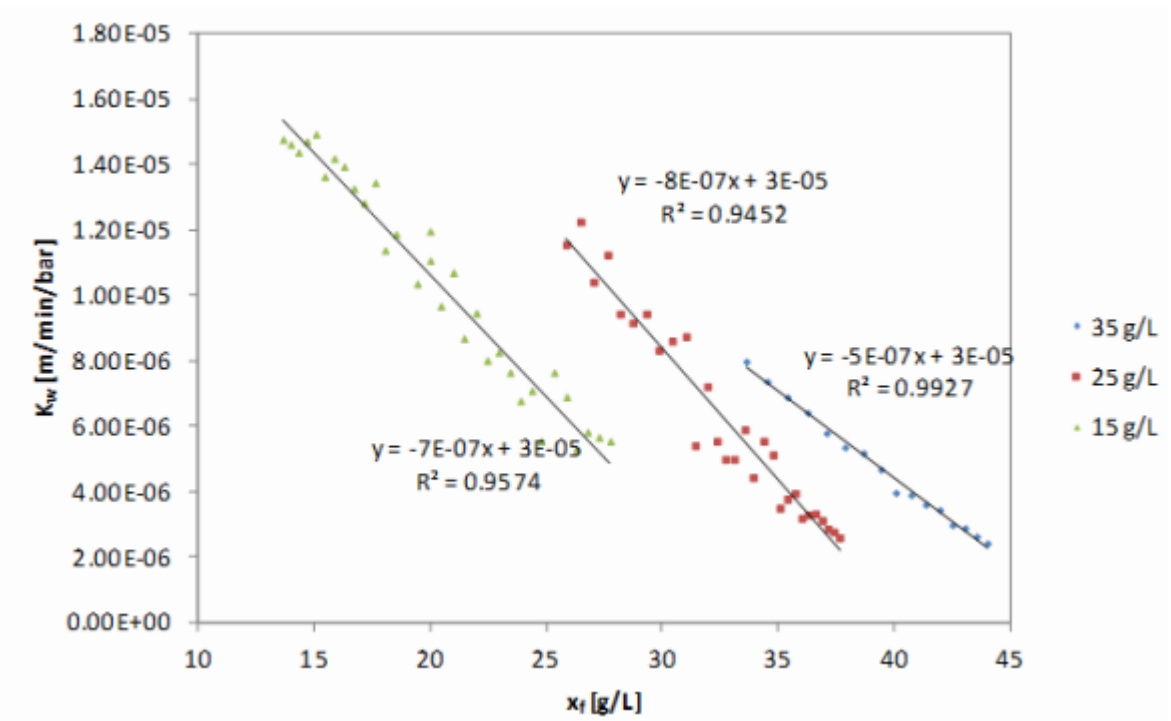

Figure 16. Water permeability trend with feed salinity at *P=45* bar.

5. Concentration polarization

The term concentration polarization refers to the salinity gradient of salts on the high-pressure side of the reverse osmosis membrane surface created by the re-dilution of salts left behind as water permeates through the membrane itself. The salinity in this boundary layer has a higher value than the salinity of the bulk water which affects the performance of the RO process, (Meares, 1976) by increasing the osmotic pressure at the membrane surface leading to reduced flux, increased salt leakage and it favors scale development.

As suggested by Kennedy *et al.* (1974), a material balance within the mass-transfer boundary layer near the membrane wall, between the solute carried to the membrane by convection and the solute carried away by diffusion, gives an expression that quantifies concentration polarization.

$$CP = \frac{x_w - x_p}{x_b - x_p} = \exp\left(\frac{M_p}{60000\,k\,A}\right) \tag{28}$$

Where x_w is the concentration at the membrane wall, x_p the permeate salinity, x_b the brine salinity and k the mass transfer coefficient.

The mass-transfer coefficient may be estimated using an appropriate empirical mass-transfer expression. For fully developed laminar and turbulent flow regimes, Belfort gives the two following relations, (Belfort, 1984):

$$Sh = \frac{kd_h}{D} = 1.86\left(\frac{Re\,Sc\,d_h}{L}\right)^{0.33} \quad \text{(laminar)} \tag{29}$$

$$Sh = \frac{kd_h}{D} = 0.04 Re^{0.75} Sc^{0.33} \quad \text{(turbulent)} \tag{30}$$

Where *Sh*, *Re* and *Sc* are the Sherwood, Reynolds (Equation 22) and Schmidt (Equation 19) numbers respectively, *L* the length of the membrane and d_h the hydraulic diameter of the flow channel.

Figure 17 shows how *CP* varies with time for an initial feed salinity of 35 g/L at pressures of 40 and 45 bar. Correspondingly, Figure 18 shows a graph of M_p against *CP*. It is possible to see from this data how at higher pressures the concentration polarization phenomenon is more pronounced due to the increase in driving force.

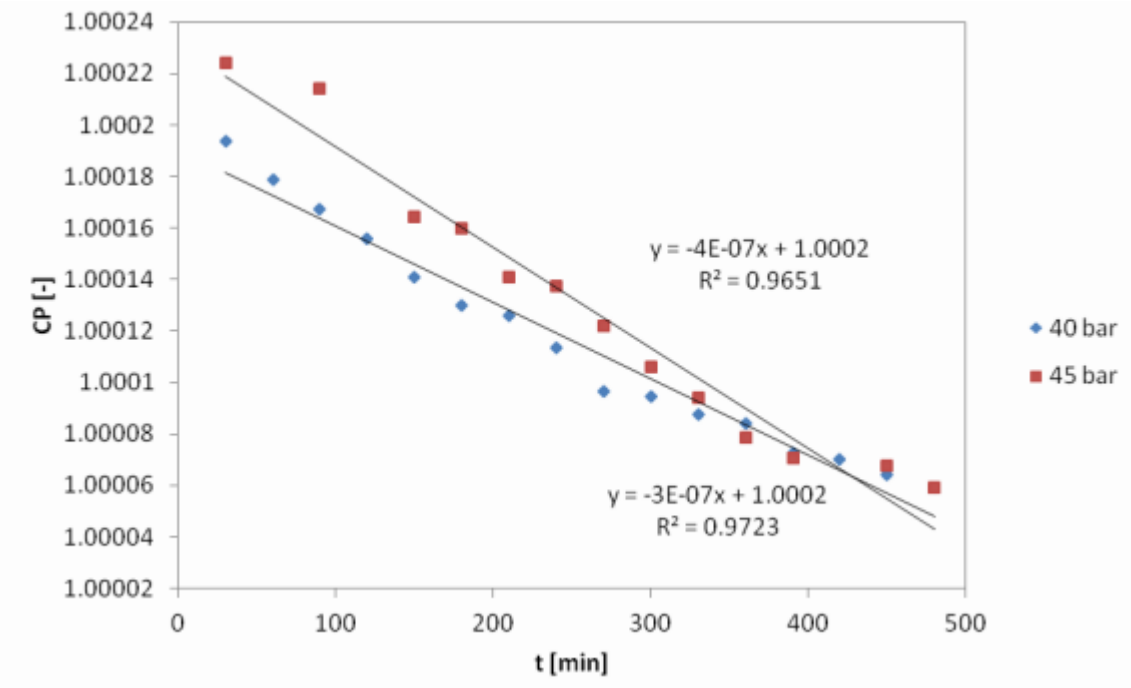

Figure 17. Concentration polarization trend with x_{f0} =35 g/L.

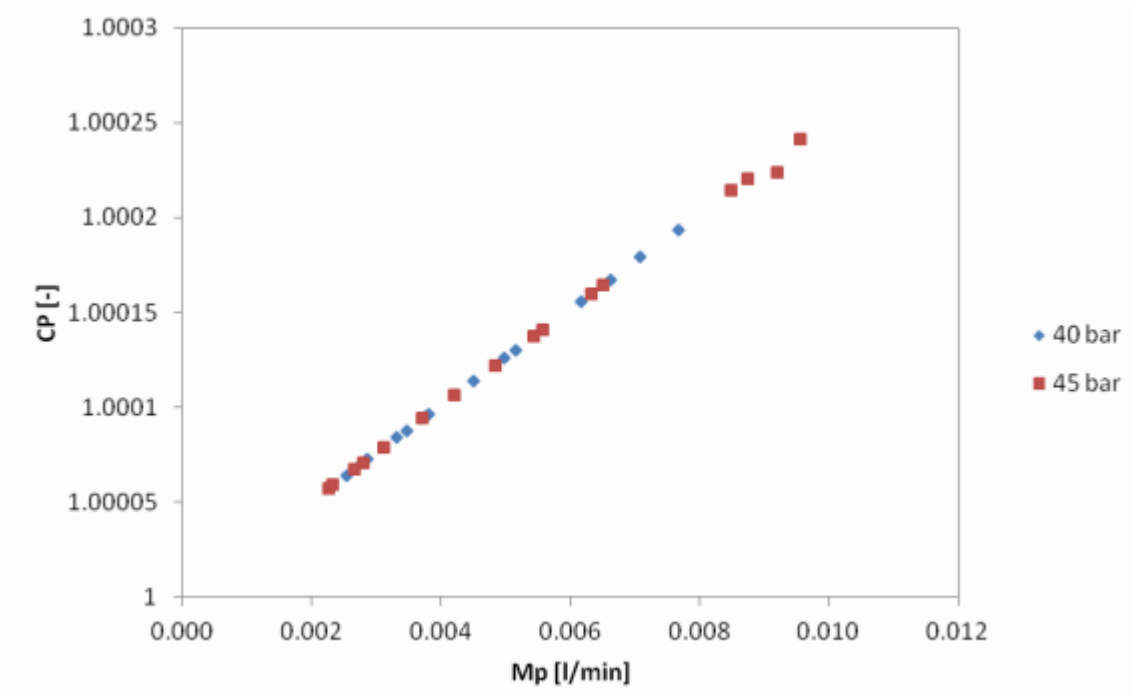

Figure 18. Concentration polarization trend with permeate flux at x_{f0}=35 g/L.

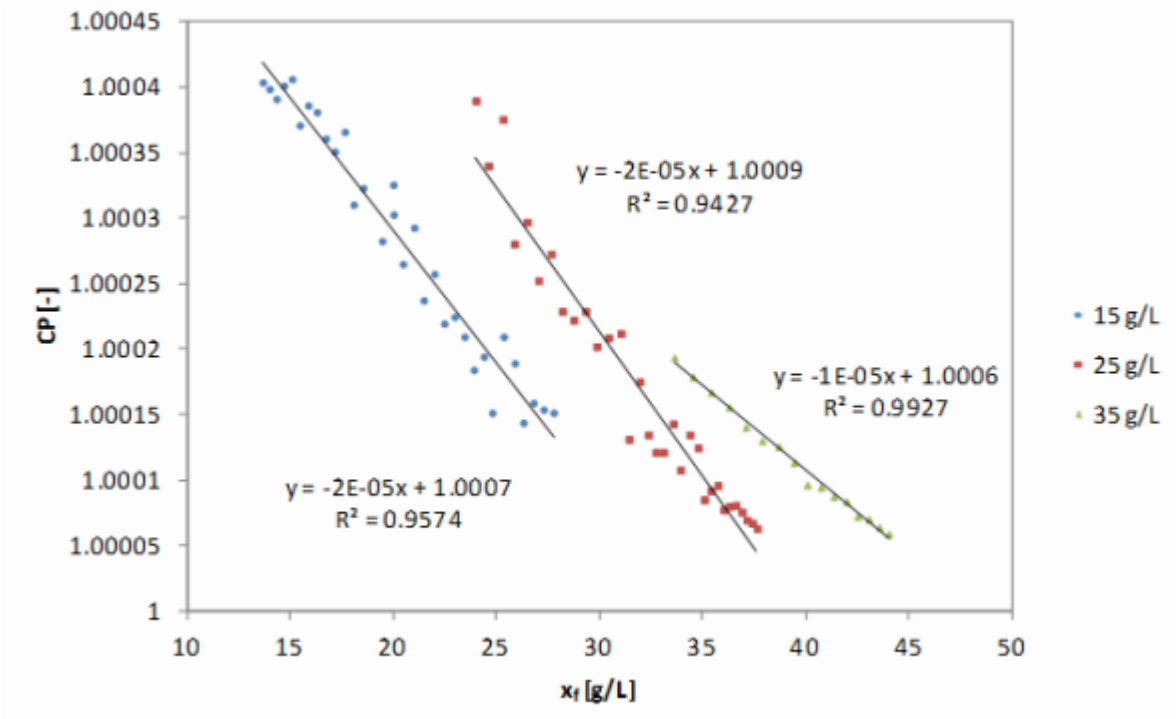

Figure 19. Feed salinity influence on concentration polarization at *P=45* bar.

The variation of *CP* with feed salinity for different initial salinities is shown in Figure 19. Results are plotted for an operating pressure of 45 bar and similar trends were found at 40 bar. In an ideal case, one would expect all the data points to fall on a single line. However, as mentioned earlier in Section 3.2, with x_{f0}=15, the *CP* effect becomes increasingly more pronounced as feed salinity increases and this causes a decay in the permeate flow (Figure 10). Also, in this case it is possible to make an interesting observation. In the study with x_{f0}=25, the *CP* value is higher compared to *CP* at x_f=30 (with x_{f0}=15) (see Figure 17), which consequently decreases the value of x_p (see Figure 9). Similarly, the behaviour of the profiles with x_{f0}=35 and x_{f0}=25 can be explained. Again, to the best of authors' knowledge, these types of observation have not yet been reported in the literature yet.

6. Salt transport

As suggested by El-Dessouky and Ettouney (2002), the rate of salt flow through the membrane can be defined by:

$$J_s = K_s\left(\bar{x} - x_p\right)A \tag{31}$$

Where K_s is the salt permeability coefficient and x_p the permeate salinity. The average salinity is defined as:

$$\bar{x} = \frac{M_f x_f + M_b x_b}{M_f + M_b} \tag{32}$$

The permeate salinity depends on the relative rates of water and salt transport through reverse osmosis membrane:

$$x_p = \frac{J_s}{M_p} \tag{33}$$

The fact that water and salt have different mass transfer rates through a given membrane creates the phenomenon of salt rejection. No membrane is ideal in the sense that it absolutely rejects salts; rather, the different transport rates create an apparent rejection.

The salt permeability coefficient trends are shown in Figures 20 and 21. In the former, it is possible to see the influence of the initial feed salinity at a constant pressure of 40 bar. Higher values of x_{f0} correspond to smaller K_s because the separation becomes more difficult. This behaviour confirms the results of Voros *et al.* (1996) where the dependence of pressure on the salt coefficient is plotted and a higher operating pressure produces higher K_s. As for the water permeability constant, it is possible to obtain a correlation that describes the dependence of the feed salinity on K_s. Results are plotted in Figure 22 for a constant pressure of 40 bar.

Figures 23 and 24 show the salt flow through the membrane as a function of time. The former shows the influence of the initial feed salinity whilst the latter displays the influence of the operating pressure.

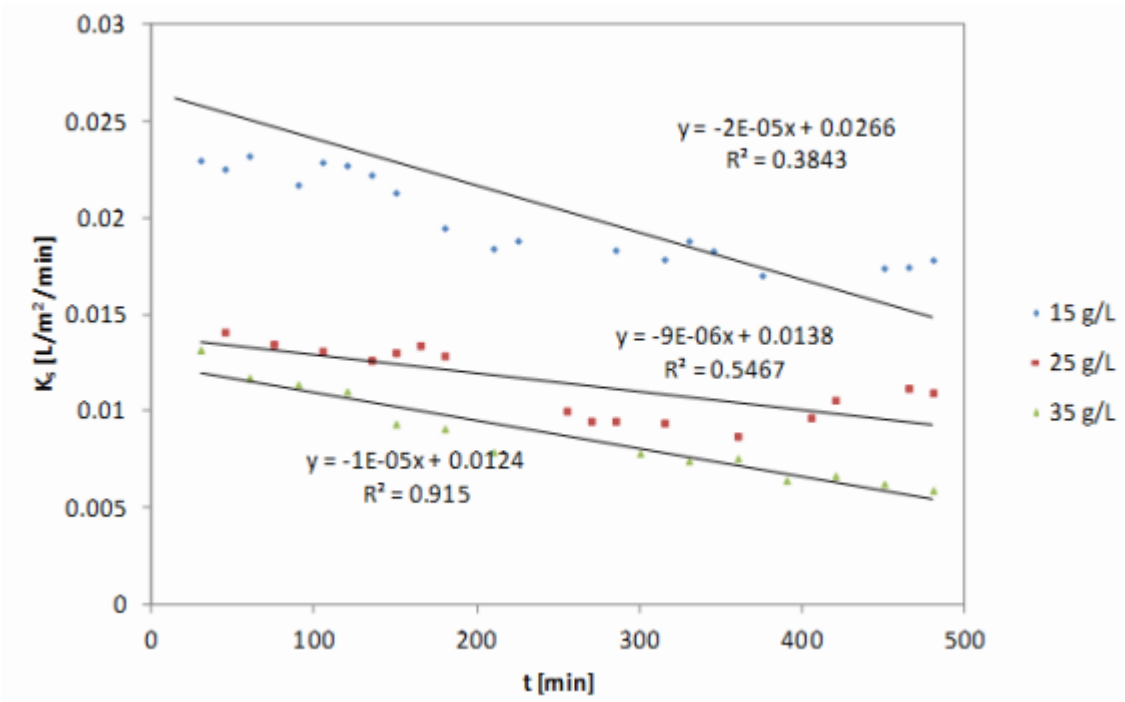

Figure 20. Salt permeability coefficient trend at *P*=40 bar.

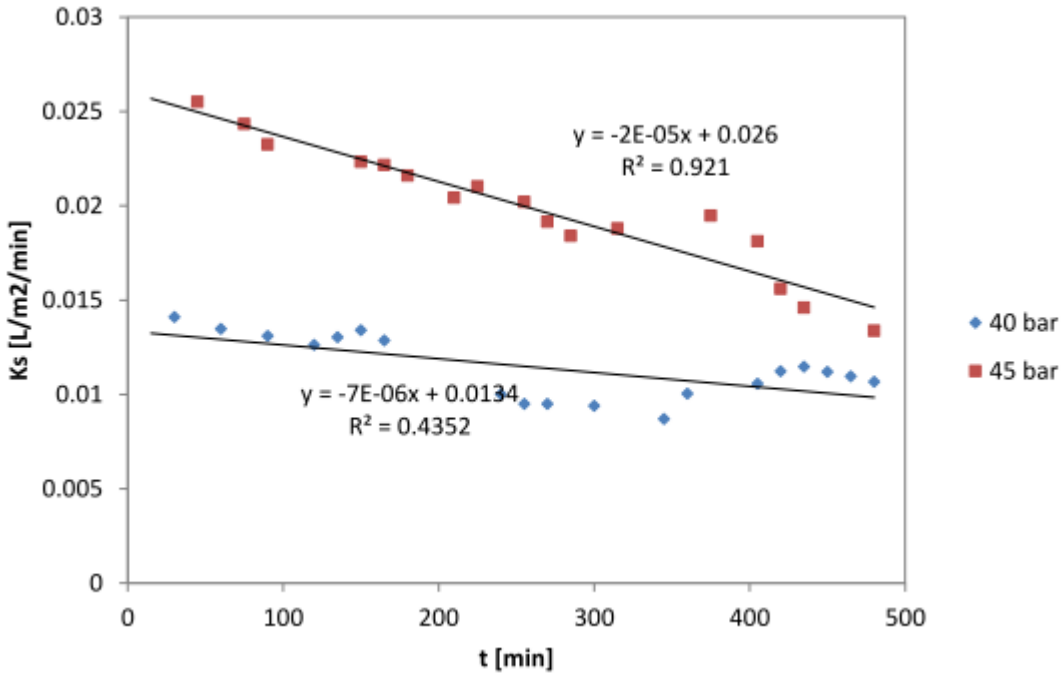

Figure 21. Salt permeability coefficient at x_{f0}=25 g/L.

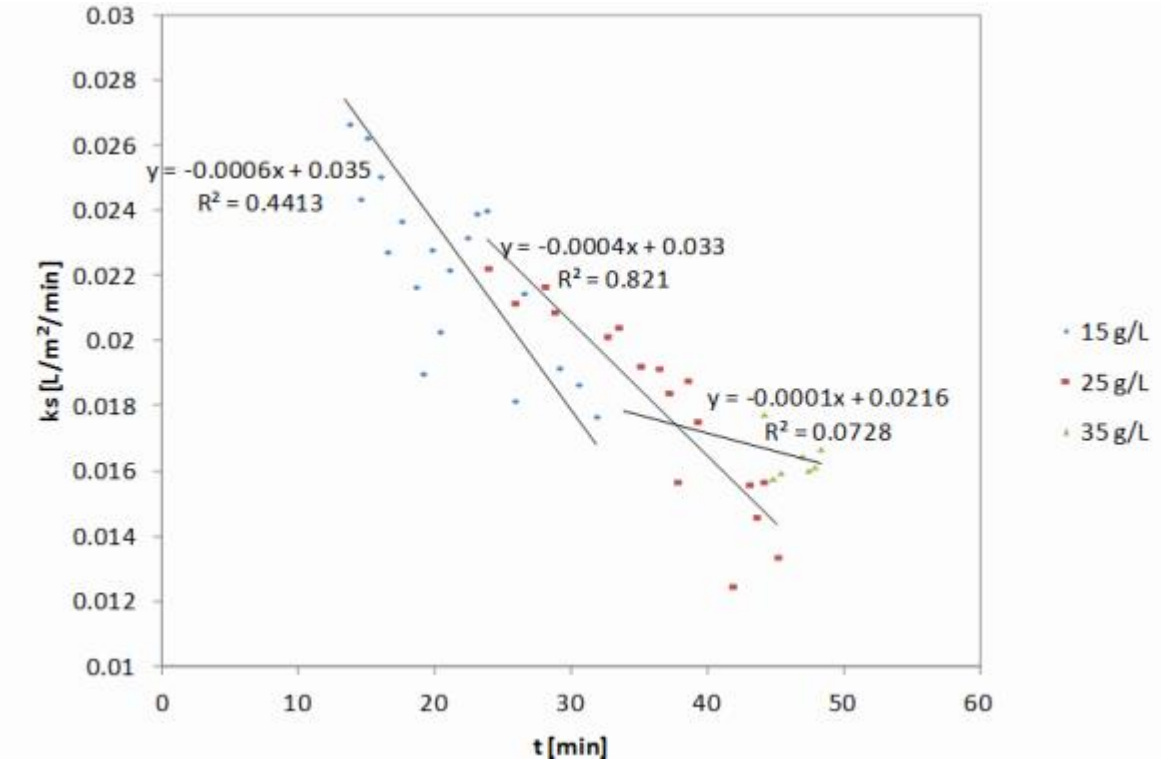

Figure 22. Salt permeability trend with feed salinity at *P*=40 bar.

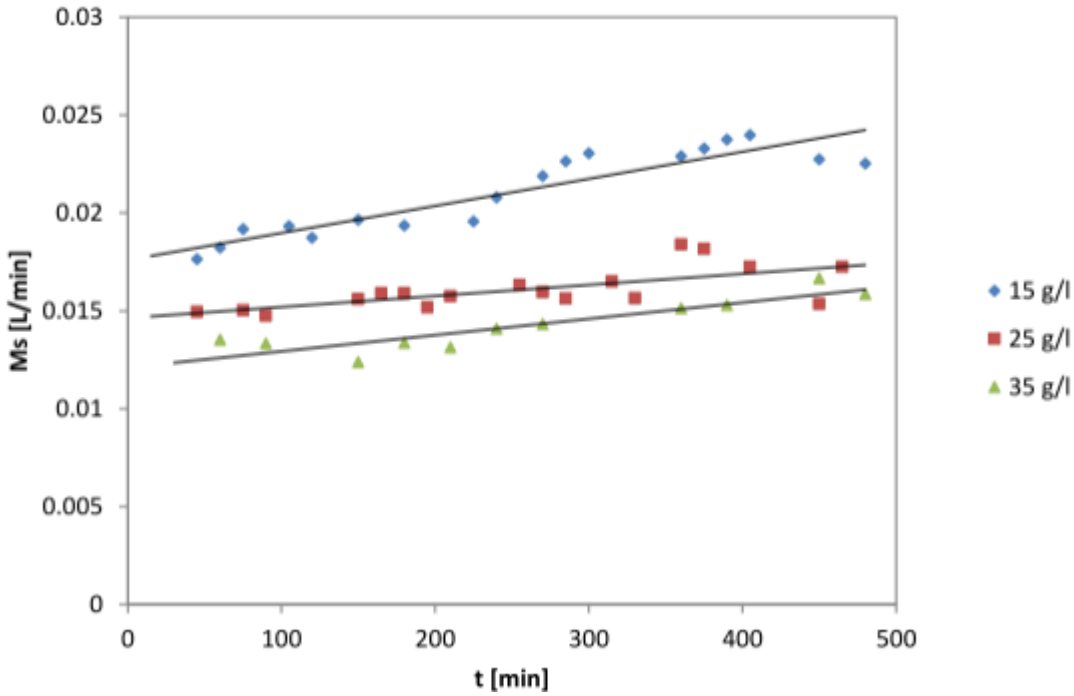

Figure 23. Salt flow trend at *P=45* bar.

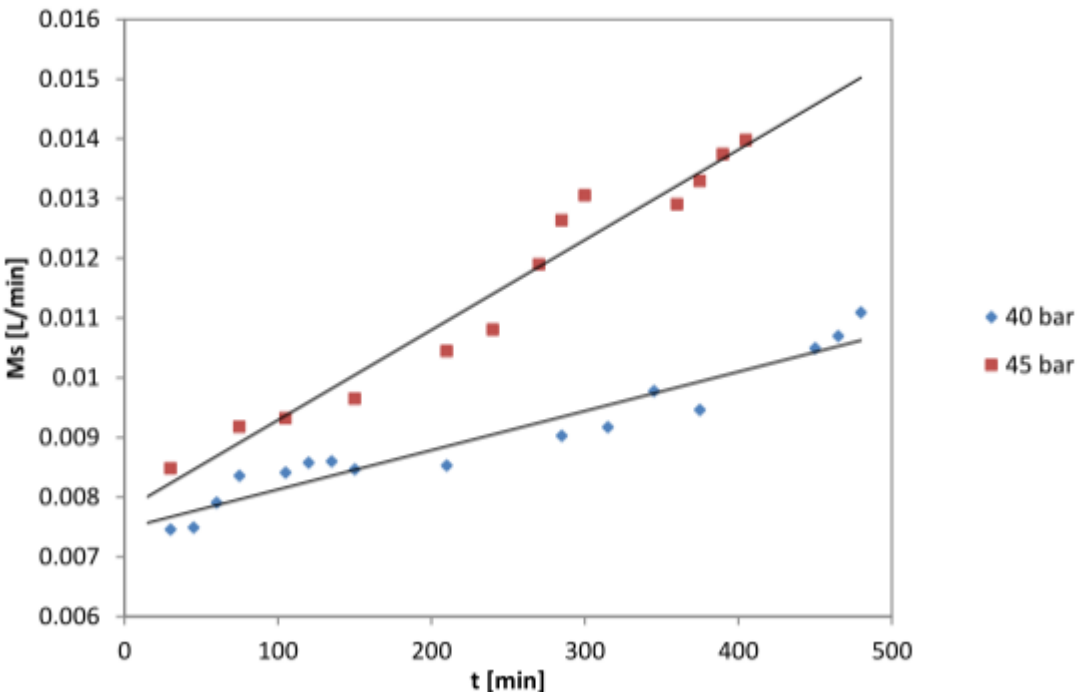

Figure 24. Salt flow trend with x_{f0}=*15* g/L.

7. Process modelling

With reference to Figure 2, the mass and salt balances for the feed tank can be written as follows:

$$\frac{d\left(Q_f\right)}{dt} = -M_p \tag{34}$$

$$\frac{d\left(Q_f x_f\right)}{dt} = -M_p x_p \tag{35}$$

As for the feed tank, it is possible to write two equations of mass and salt balances to characterize the permeate feed tank:

$$\frac{d\left(Q_{p_t}\right)}{dt} = M_p \tag{36}$$

$$\frac{d\left(Q_{p_t} x_{p_t}\right)}{dt} = M_p x_p \tag{37}$$

These four differential equations, coupled with one of the two theories (El-Dessouky and Ettouney, 2002; Meares, 1976) previously discussed (Section 4.1 and 4.2) to describe the RO system, give a complete description of the plant.

Calculating the degree of freedom of the system is one of the steps to carry out the simulation of the process. Table 2 shows the number of degrees of freedom for both the models. Both models have 2 degrees of freedom (DoF) and it is possible to look for literature values of the water and salt permeability constants. By selecting values of water and salt permeability constants, the DoF reduce to zero and it is then possible to solve the system of equations describing the RO plant and validate the model by comparing these results with the experimental data.

Table 3 shows the parameters specified for both models. Note that K_w and K_s values (for non-fouled membrane) are taken from Voros et al. (1996) (tubular membrane, P=25, 30, 35 and 40 bar).

Figures 25 and 26 show the results for both models (for x_{f0}=35) and it is plain to see that there is a mismatch between experimental results and calculated results. This is, partly due to some measurement errors and the fact that constant values for K_w and K_s are used. In reality, K_w and K_s are not constant and it is thus necessary to incorporate in the model the dependence of the feed salinity from these parameters. From the experimental results (Figures 13, 16, and 22), a linear regression is performed in order to obtain two expressions of water and salt permeability constants as a function of x_f. Tables 4, 5, and 6 show the correlations for each initial condition (x_{f0}) with the respective correlation coefficients, R^2. It is possible to see that after implementing this correction (Figures 27 and 28 (for $x_{f0}=35$)), there is good agreement between experimental and predicted values, especially for El-Dessouky and Ettouney (2002). Same results were found for x_{f0}=25 and x_{f0}=15. It might be due to the fact that the experimental conditions including the type of membrane used in this work can be described better with El-Dessouky and Ettouney model than the Meares model and that the model assumptions considered by the former model matches the experimental conditions of this work better than the latter model.

Table 2. Degrees of freedom.

	m	n	d	Specified parameters	Remaining specifications
El-Dessouky and Ettouney [2002]	24	15	9	M_f, ΔP, A Q_f^0, x_f^0, Q_{pt}^0, x_{pt}^0	2
Meares [1976]	33	21	12	M_f, ΔP, A, T, α, d_h Q_f^0, x_f^0, Q_{pt}^0, x_{pt}^0	2

Table 3. Parameter values.

Settings	Initial conditions	Literature values
Mf = 18 [l/min]	Q_f^0 = 8 [l]	K_w=2.4E-5 [m^3/min/m^2/bar]
ΔP = 40 [bar]	x_f^0 = 35 [g/L]	K_s=0.0237 [l/min/m^2]
A = 0.024 [m^2]	Q_{pt}^0 = 1.E-10	
T = 23-33 [°C]	x_{pt}^0 = 1.E-10	
α = 2 [-]		
d_h = 0.01635 [m]		

Table 4. Water and salt permeability correlations for x_{f0}=35 g/L. (this work)

K_w [m^3/min/m^2/bar]	Based on El-Dessouky and Ettouney model	Based on Meares model
Equation	$K_w = -1.0 \times 10^{-6} x_f + 6.0 \times 10^{-5}$	$K_w = -5.0 \times 10^{-7} x_f + 3.0 \times 10^{-5}$
R^2	0.9687	0.9927
K_s [l/m2/min]	El-Dessouky and Ettouney	Meares
Equation	$K_s = -3.0 \times 10^{-4} x_f + 0.0224$	$K_s = -3.0 \times 10^{-4} x_f + 0.0224$
R^2	0.8802	0.8802

Table 5. Water and salt permeability correlations for x_{f0}=*25* g/L. (this work)

K_w [$m^3/min/m^2/bar$]	Based on El-Dessouky and Ettouney model	Based on Meares model
Equation	$K_w = -1.0 \times 10^{-6} x_f + 6.0 \times 10^{-5}$	$K_w = -8.0 \times 10^{-7} x_f + 3.0 \times 10^{-5}$
R^2	0.9516	0.9452
K_s [$l/m^2/min$]	El-Dessouky and Ettouney	Meares
Equation	$K_s = -2.0 \times 10^{-4} x_f + 0.0195$	$K_s = -2.0 \times 10^{-4} x_f + 0.0195$
R^2	0.9029	0.9029

Table 6. Water and salt permeability correlations for x_{f0}=*15* g/L. (this work)

K_w [$m^3/min/m^2/bar$]	Based on El-Dessouky and Ettouney model	Based on Meares model
Equation	$K_w = -9.0 \times 10^{-7} x_f + 4.0 \times 10^{-5}$	$K_w = -7.0 \times 10^{-7} x_f + 3.0 \times 10^{-5}$
R^2	0.9574	0.9574
K_s [$l/m^2/min$]	El-Dessouky and Ettouney	Meares
Equation	$K_s = -4.0 \times 10^{-4} x_f + 0.0293$	$K_s = -4.0 \times 10^{-4} x_f + 0.0293$
R^2	0.9173	0.9173

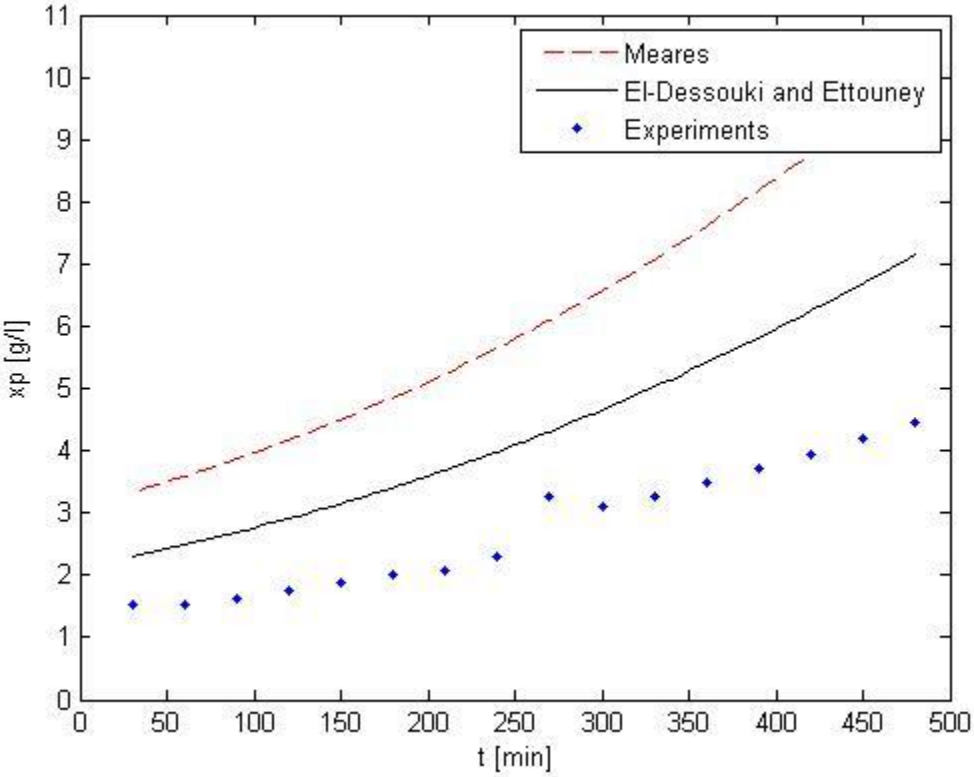

Figure 25. Permeate salinity trends Matlab calculations (x_{f0}=*35 g/L*).

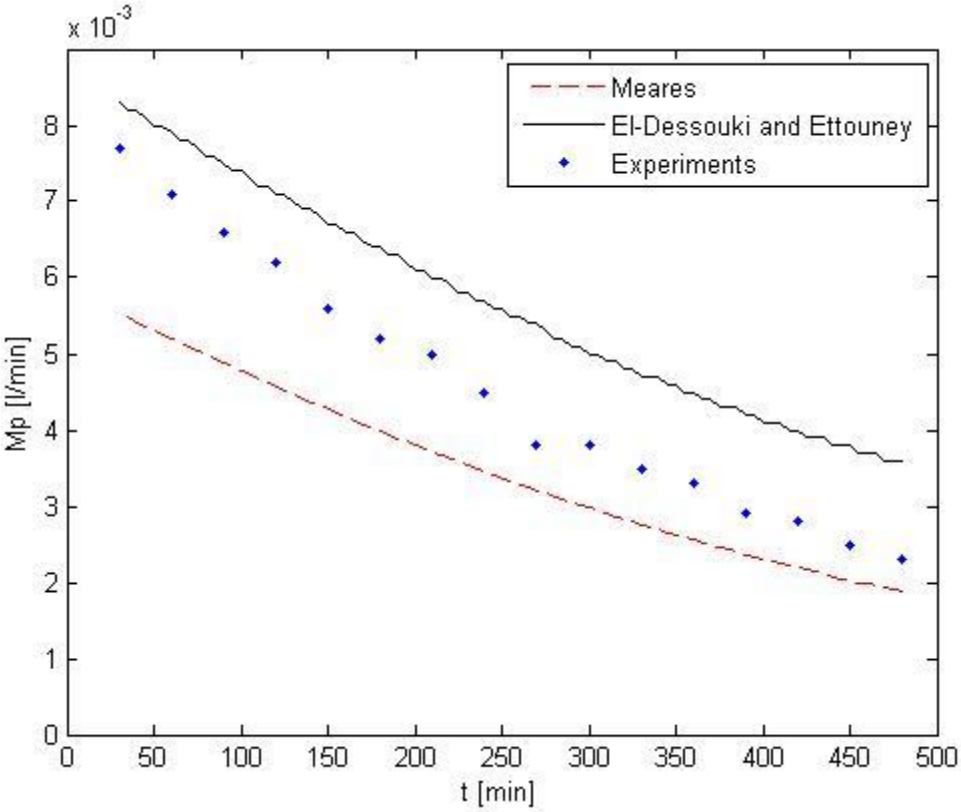

Figure 26. Permeate flux trends Matlab calculations (x_{f0}=*35 g/L*).

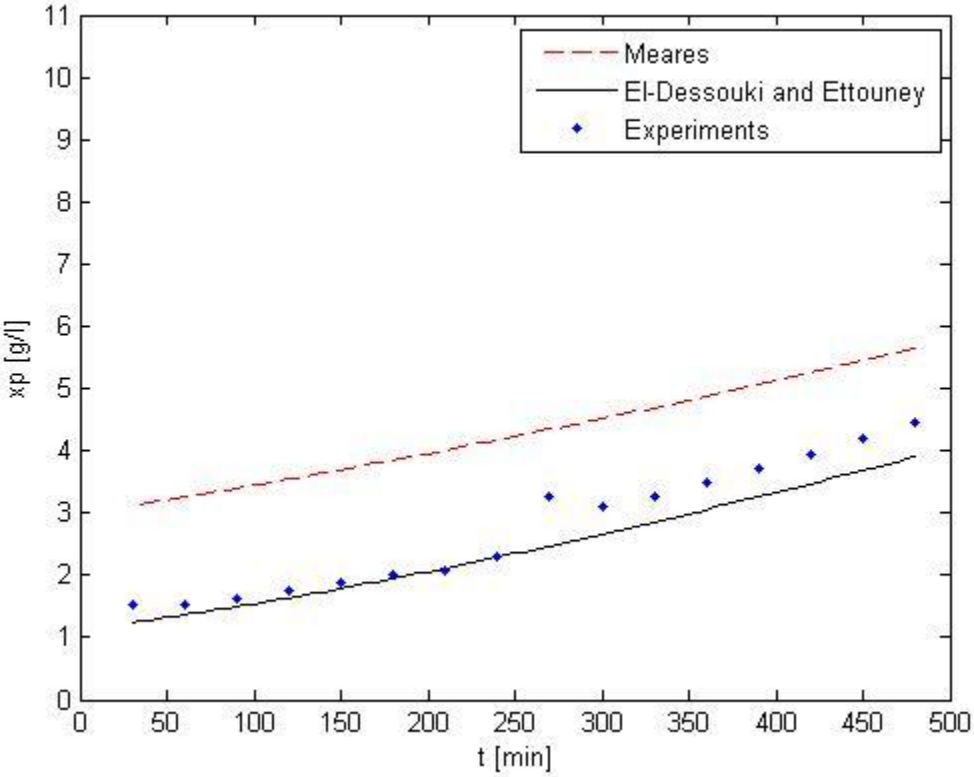

Figure 27. Permeate salinity trends with feed salinity dependence on water and salt permeability (x_{f0}=*35 g/L*).

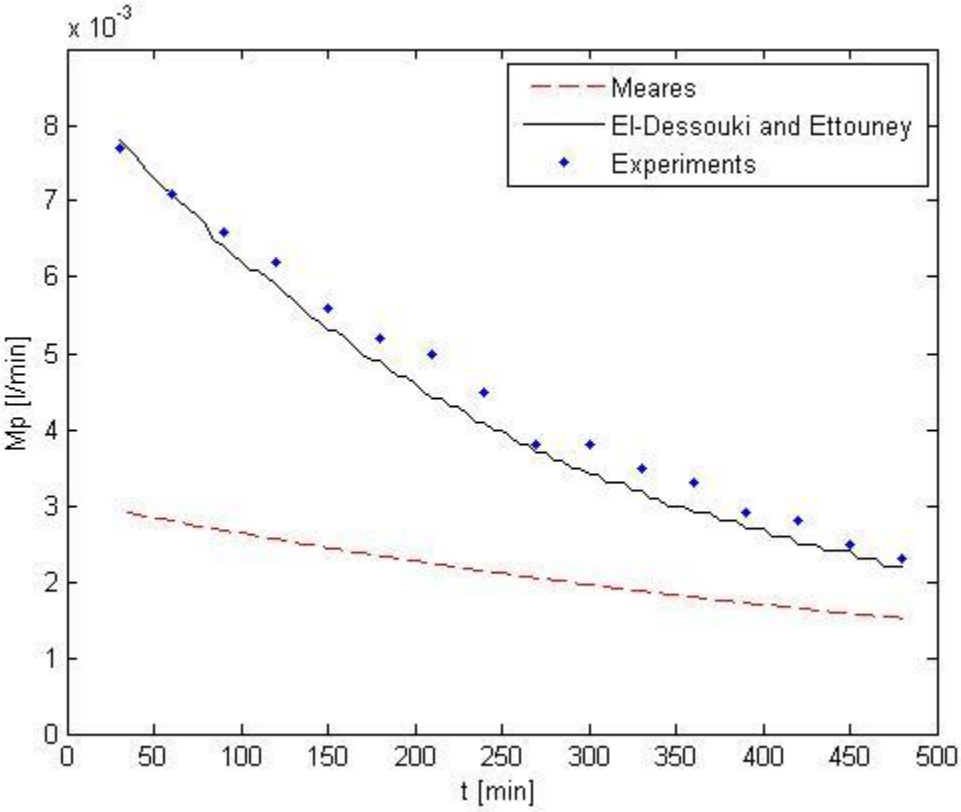

Figure 28. Permeate flux trends with feed salinity dependence on water and salt permeability (x_{f0}=*35 g/L*).

8. Constant feed tank salinity

The RO plant was run at constant feed tank salinity in order to observe the difference with the batch configuration. In the experimental set up, since it was not possible to disconnect the brine recirculation to the feed tank, through a mass balance at discrete time interval, fresh water was added to the feed tank to keep the salinity constant. It is possible to see from Figure 29 that this method was successful as the x_f trend is almost constant with the time. In Figures 28 and 29 results are plotted for an operating pressure of 40 bar and an initial feed salinity of 35 g/L (batch system) and constant feed salinity of 35 g/L. As expected, *Mp*, *xp* and K_w remain constant for constant feed salinity and since the plant was run for only 8 hours, it was not possible to see appreciable fouling.

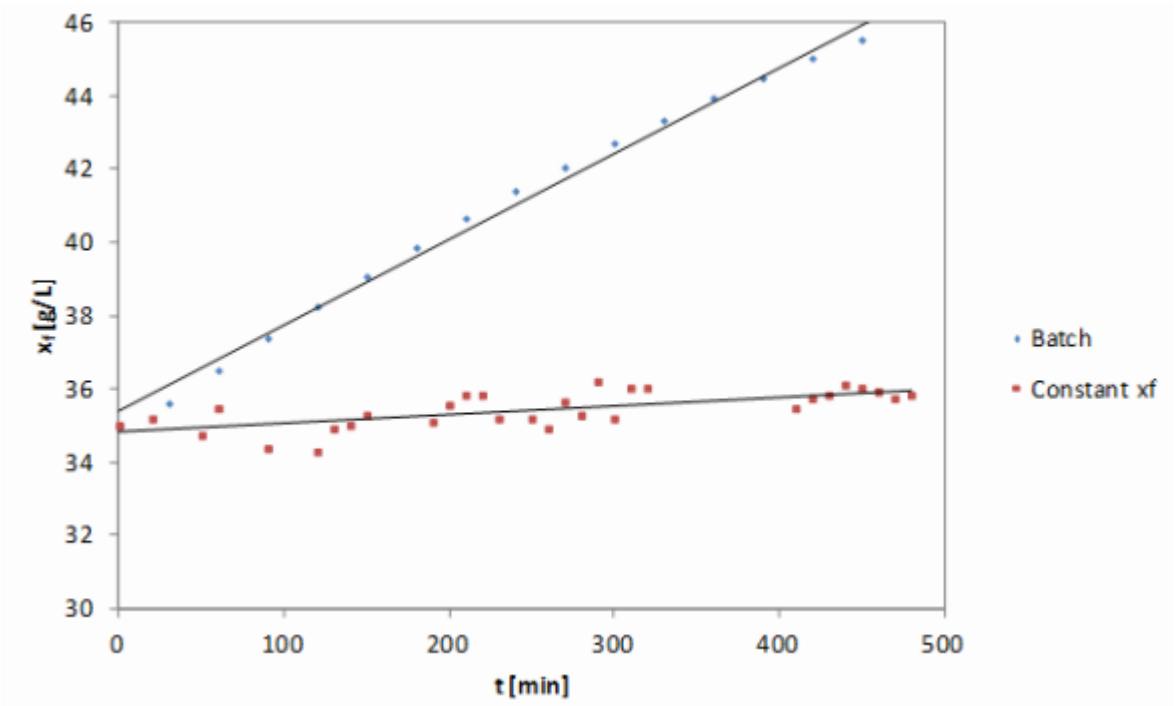

Figure 29. Feed tank salinity trend

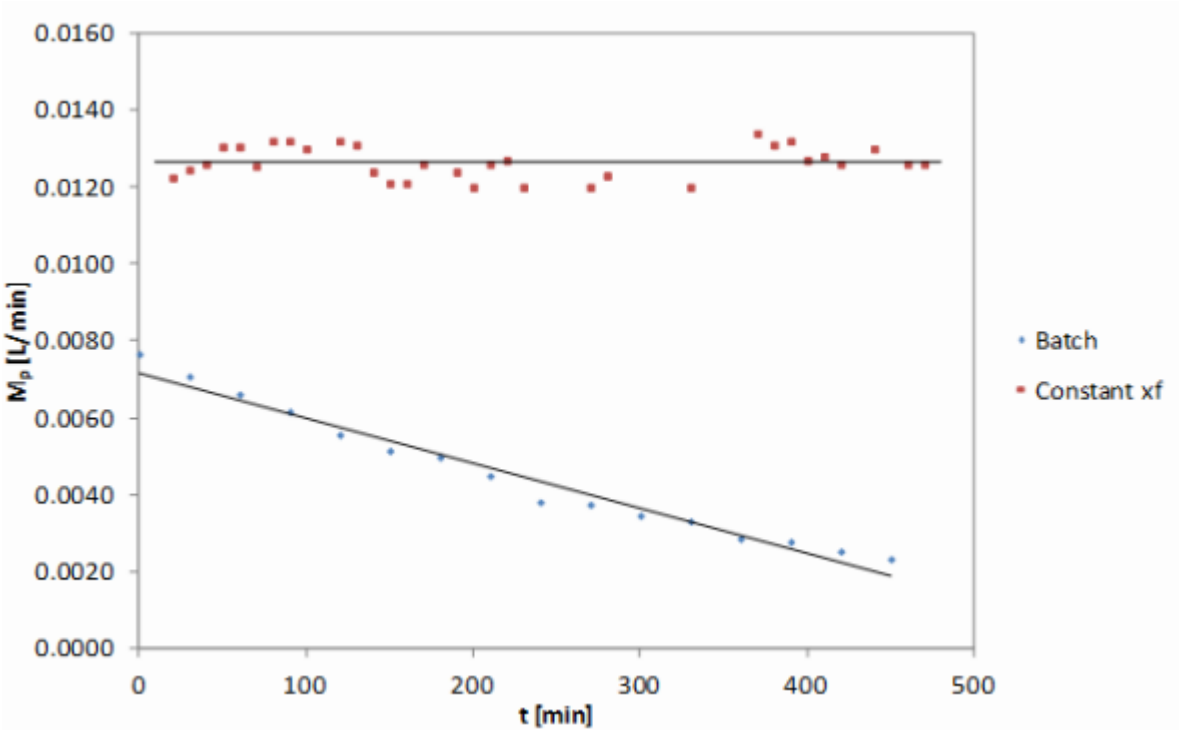

Figure 30. Permeate flux trend for batch and continuous running.

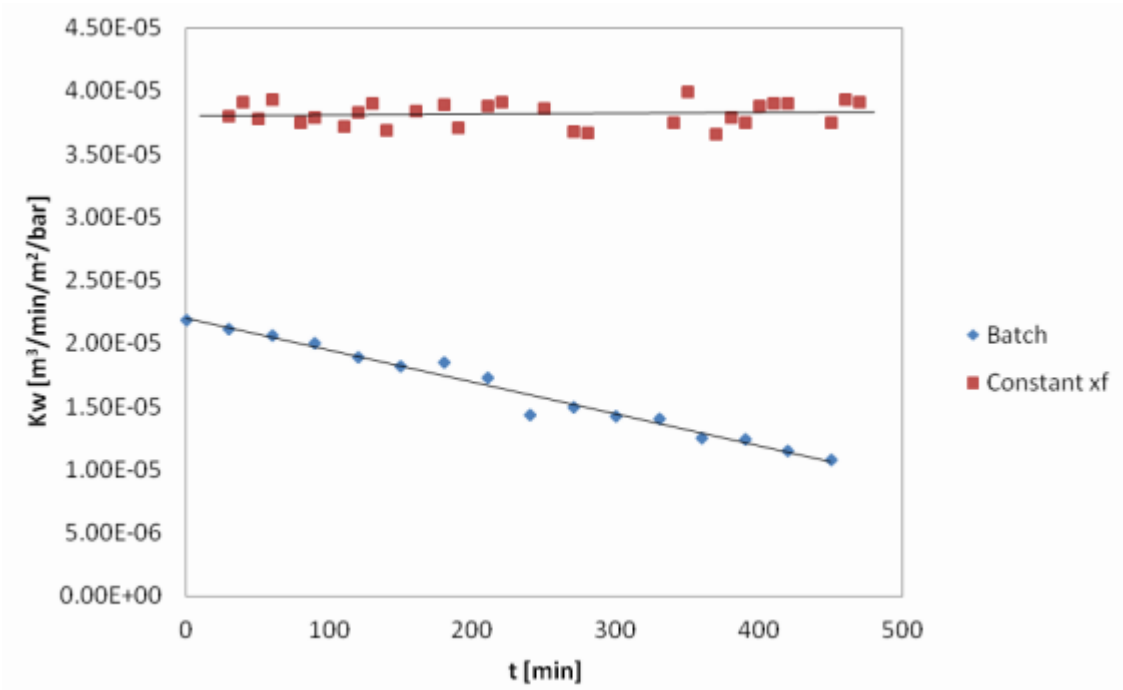

Figure 31. Water permeability trend for batch and continuous running.

9. Conclusions

This paper presented, characterized and modelled a batch reverse osmosis desalination plant. The batch mode of operation is achieved by recirculating the brine stream which increases the feed tank salinity continuously, allowing in-depth investigation of the effect of feed salinity on the water permeability constant which was never the focus in the past. In addition, experiments were carried out for different operating pressures to investigate if the effect of pressure on the water permeability constant remains the same observed in the past (while keeping feed salinity constant). The behavior of other important process parameters such as concentration polarization, salt transport, etc. were also studied. Finally, the experimental data were validated against two literature RO models.

Permeate flux was found to increase with increasing pressure and for lower salinity whereas permeate salinity was found to increase for higher pressure and salinity. An important observation was made by studying the permeate salinity trends with feed salinity. It is found that the concentration polarization phenomena can influence these trends and for different starting conditions *i.e.* different initial feed salinities, the values of the permeate salinity at a chosen feed salinity are different. In the literature there is no evidence of these dependencies. Water permeability constant was evaluated as a function of changing feed salinity and pressure from the collected experimental data and using two models from the literature. A strong pressure dependence of the water permeability constant was observed in line with earlier observations. Interestingly, strong salinity dependence of the water permeability constant is also observed which has been neglected or ignored in the literature by authors who studied this aspect of the process and considered only the water permeability decay with the time due to the fouling phenomena. To be absolutely sure of our findings, we carried out an additional experiment at constant feed salinity. This experiment confirms earlier observations reported in the literature and at the same time strengthens our new findings.

In addition, the salt transport mechanism was studied in terms of mass flow of salt that passes though the membrane and the salt permeability constant. Interestingly, a strong feed salinity dependence on the latter was found, which has not yet been reported in the literature.

The batch RO process has been modelled by means of a differential-algebraic equations system. Initially, constant values of water and salt permeability were taken from the literature and a significant difference was found between experimental and simulated results. When water and salt permeability constants as functions of salinity are introduced in the model, results improved significantly for El-Dessouky and Ettouney (2002) model, proving that the experimental process considered in this work can be adequately described by this model.

Finally, it is worth observing that feed salinity plays an important role in deciding the optimal RO network configuration and a number of operating parameters as observed by Lu et al. (2007) and Sassi and Mujtaba (2012) to reduce the cost of production of water ($0.22-$1.34) per m^3 of freshwater produced. However, in all these studies constant (concentration independent) water and salt permeability constants were used. Our work will certainly have implications on the design and operation of RO desalination processes and on the cost of production of water which will be explored in future.

10. Notation

ΔP	Net hydraulic pressure differential across the membrane, bar
A	Membrane area, m^2
CP	Concentration polarization factor, -
C_1	Conversion factor (from m^3/min to L/min) = 1000
d	Degrees of freedom, -
D	Feed diffusivity, m^2/s
d_h	Hydraulic diameter, m
j	Chilton-Colburn factor, -
J_s	Salt flow through the membrane, g/min
k	Mass transfer coefficient, m/s
K_s	Salt permeability coefficient, L/m^2/min
K_w	Water permeability constant, m^3/min/m^2/bar
L	Membrane length, m
M	Density temperature factor, °C
m	Total number of variables, -
M_b	Brine flow rate, L/min
M_f	Feed flow rate, L/min
M_p	Permeate flow rate, L/min
$\underline{n}$	Total number of equations, -
Q_f	Feed quantity, L
Q_p	Permeate quantity, L
Q_{pt}	Total permeate quantity, L
R	Gas constant, atm/m^3/kmol/K
Re	Reynolds number, -
R_j	Salt rejection, -
Sc	Schmidt number, -
Sh	Sherwood number, -
T	Operating temperature, °C
t	Time, min

$\underline{u}$	Brine velocity, m/s
$\underline{x}$	Average salinity, g/L
x_b	Brine salinity, g/L
x_f	Feed salinity, g/L
x_p	Permeate salinity, g/L
x_{pt}	Total permeate salinity, g/L
x_w	Wall salinity, g/L
α	Number of ions produced on complete dissociation of one molecule of electrolyte, -
$\Delta\pi$	Net osmotic pressure differential across the membrane, bar
μ	Feed dynamic viscosity, kg/s/m
v	Feed kinematic viscosity, m^2/s
$\underline{\pi}$	Average osmotic pressure on the feed side, bar
π_b	Brine osmotic pressure, bar
π_f	Feed osmotic pressure, bar
π_p	Permeate osmotic pressure, bar
ρ	Feed density, kg/m^3

References

Al-Bastaki, N., & Abbas, A. (2004). Long-term performance of an industrial water desalination plant, *Chemical Engineering Processing*, *43* 555-558.

Altaee, A. (2012). Computational model for estimating reverse osmosis system design and performance: Part-one binary feed solution, *Desalination*, *291* 101-106.

Barello, M., Manca, D., Patel, R. & Mujtaba, I.M. (2014). Neural network based correlation for estimating water permeability constant in RO desalination process under fouling, *Desalination*, *345* 101-111.

Belfort, G. (1984). Synthetic Membrane Process: Fundamentals and Water Applications, Academic Press Inc., New York.

Djebedjian, B., Gad, H., Khaled, I. & Rayan, M.A. (2008). Optimisation of reverse osmosis desalination system using genetic algorithms technique, Twelfth International Water Technology Conference, IWTC12, Alexandria, Egypt.

Du, Y., Xie, L., Liu, J., Wang, Y., Xu, Y. & Wang, S. (2014). Multi-objective optimization of reverse osmosis networks by lexicographic optimization and augmented epsilon constraint method, *Desalination*, *333* 66-81.

El-Dessouky, H.T. & Ettouney, H.M. (2002). Fundamentals of sea water desalination, Amsterdam: Elsevier Science.

Geraldes, V.M., Semiao, V.A. & de Pinho, M.N. (2001). Flow and mass transfer modelling of nanofiltration. *J Membr Sci*, *191* 109–128.

Kennedy, T.J., Merson, R.L., & McCoy, B.J. (1974). Improving permeation flux by pulses reverse osmosis, *Chemical Engineering Science*, *29* 1927-1931.

Kim, J., Park, M., Snyder, S.A. & Kim J.H. (2013). Reverse osmosis (RO) and pressure retarded osmosis (PRO) hybrid processes: Model-based scenario study. *Desalination 322* 121-130.

Lu, Y.Y., Hu, Y.D., Zhang, X.L., Wu, L.Y. & Liu, Q.Z., (2007). Optimum design of reverse osmosis system under different feed concentration and product specification, Journal of membrane science, *287*, 219-229.

Meares, P. (1976). Membrane separation process, Elsevier Scientific, Oxford.

Pais, J.A.G.C.R., Manuel, L. & Ferreira, G.A. (2007). Performance study of an industrial RO plant for seawater desalination, *Desalination* 269-276.

Schiffler, M. (2004). Perspectives and challenges for desalination in the 21st century, *Desalination*, *165* 1–9.

Sassi, K.M. & Mujtaba, I.M. (2012). Effective Design of Reverse Osmosis Based Desalination Process Considering Wide Range of Salinity and Seawater Temperature, *Desalination 306*, 8–16

Shamel, M.M. & Chung, O.T. (2006). Drinking water from desalination of seawater: optimisation of reverse osmosis system operating parameters, *Journal of Engineering Science and Technology*, *1*(2) 203-211.

Stover, R. (2011). CCD Starts a New Generation for RO, Desalination and Water Reuse, November-December, 34 – 35.

Tarquin, A. & Delgado, G. (2012). Concentrate Enhanced Recovery Reverse Osmosis: A New Process for RO Concentrate and Brackish Water Treatment, Proceedings of the American Institute of Chemical Engineers Meeting in Pittsburg, PA, (2012) paper number 272277, October N.G. Voros, Z.B.

Maroulis, D. Marinos-Kouris, (1996). Salt and sea water permeability in reverse osmosis membranes, *Desalination*, *104* 141-154.

Wardeh, S. & Morvan. H.P. (2008). CFD simulations of flow and concentration polarization in spacer-filled channels for application to water desalination, Chemical Engineering Research and Design, 86 1107–1116.

Wilf, M. & Klinko, K. (1994). Performance of commercial seawater membranes, *Desalination*, *96* 465-476.

Zhu, M., El-Halwagi, M.M. & Al-Ahmad, M. (1997). Optimal design and scheduling of flexible reverse osmosis networks, *Journal of Membrane Science*, *129* 162-174.